Sorting of cadherin-catenin-associated proteins into individual clusters

Regina B. Troyanovsky[1], Alina P. Sergeeva[2], Indrajyoti Indra[1], Chi-Shuo Chen[1,a], Rei Kato[1], Lawrence Shapiro[3], Barry Honig[2,3,4b], and Sergey M. Troyanovsky[1b]

[1]Department of Dermatology and Cell & Developmental Biology, Northwestern University, The Feinberg School of Medicine, Chicago, IL 60611

[2]Department of Systems Biology, Columbia University Medical Center, New York, NY 10032, USA

[3]Department of Biochemistry and Molecular Biophysics, Columbia University, New York, NY 10032, USA; Zuckerman Mind Brain Behavior Institute, Columbia University, New York, NY 10027, USA

[4]Department of Medicine, Columbia University, New York, NY 10032, USA

[a]Present address: Department of Biomedical Engineering and Environmental Sciences, National Tsing Hua University, Hsinchu City, Taiwan 300.

[b]Corresponding authors

Running title: Sorting of cadherin-associated proteins

Key words: Cadherin, Catenins, Cadherin-associated proteins, Adherens Junctions, Protein sorting

To whom correspondence may be addressed: Dr. Barry Honig
Department of Systems Biology
Columbia University
1130 St. Nicholas Ave
NY, NY 10032

Dr. Sergey Troyanovsky
Department of Dermatology
Northwestern University
The Feinberg School of Medicine,
303 E. Chicago Ave
Chicago, IL. 60611
Phone: 1-312-503-9275
Email: s-troyanovsky@northwestern.edu

Abstract

The cytoplasmic tails of classical cadherins form a multiprotein cadherin-catenin complex (CCC) that constitutes the major structural unit of adherens junctions (AJs). The CCC in AJs forms junctional clusters, "E-clusters," driven by *cis* and *trans* interactions in the cadherin ectodomain and stabilized by α–catenin/actin interactions. Additional proteins are known to bind to the cytoplasmic region of the CCC. Here we analyze how these CCC-associated proteins (CAPs) integrate into cadherin clusters and how they affect the clustering process. Using a crosslinking approach coupled with mass spectrometry, we found that the majority of CAPs, including the force-sensing protein vinculin, interact with CCC outside of AJs. Accordingly, structural modeling shows that there is not enough space for CAPs of the size of vinculin to integrate into E-clusters. Using two CAPs, scribble and erbin, as examples, we provide evidence that these proteins form separate clusters which we term "C-clusters". As proof of principle we show, using cadherin ectodomain monoclonal antibodies (mAbs), that mAb-bound E-cadherin forms separate clusters that undergo *trans* interactions. Taken together our data suggest that, in addition to its role in cell-cell adhesion, CAP-driven CCC clustering serves to organize cytoplasmic proteins into distinct domains that may synchronize signaling networks of neighboring cells within tissues.

Significance

Cadherin-catenin complexes (CCC) are a central component of adherens junctions. To produce an adhesive cell-cell contact the CCC forms clusters, "E-clusters," driven by cooperative *cis* and *trans* interactions in the cadherin ectodomain and by α–catenin/actin interactions inside cells. We analyze whether E-clustering is compatible with CCC-associated proteins (CAPs) and show that space constraints preclude the integration of many CAPs into E-clusters. Using two natural (scribble and erbin), and "artificial" (cadherin ectodomain antibodies) CAPs we provide evidence that CAPs form separate "C-clusters", unable to intermix with E-clusters. Our results thus suggest that CAP-dependent CCC clustering serves as a mechanism for sorting cellular proteins into distinct domains within cell-cell contacts.

INTRODUCTION

The core structural unit of Adherens Junctions (AJs), the cadherin-catenin complex (CCC), consists of four proteins – a classical cadherin (E-cadherin in epithelia), β-catenin, α-catenin, and p120-catenin (1-4). In the process of cell-cell adhesion, the CCC forms clusters driven by both extracellular and intracellular binding events (5-8). The clustering of cadherin molecules is essential to reinforce weak individual *trans* adhesive bonds (9-12). In addition, the continuous and fast reassembly of CCC clusters within AJs renders them both highly adhesive and yet flexible (7, 13). While the importance of CCC clustering in cell-cell adhesion was demonstrated more than two decades ago (14), many of the molecular events associated with clustering are still poorly understood. One critical question, which is the focus of this work, is the role of proteins that associate with the CCC, CAPs, and, in particular, how these proteins change the properties of CCC clusters.

While several mechanisms for CCC clustering have been proposed (12), the best characterized involves the formation of *cis* interaction between E-cadherin ectodomains. Cooperative *cis* and *trans* interactions arrange cadherin *trans*-dimers into a paracrystalline lattice with a lateral inter-cadherin (center-to-center) spacing of ~7 nm (15). The stability of these extracellular clusters is further enhanced by the binding of α-catenin to actin filaments (16-18). Accumulating data suggest that AJs consist of numerous such paracrystalline nanoclusters interspersed with less dense CCC regions (7, 15, 19-21). However, under certain conditions, cadherin clusters can be formed that do not seem to require the formation of ordered ectodomain lattices. For example, clusters are observed in cells expressing a *cis*-interaction incompetent cadherin mutant although they are less stable than wild type paracrystalline clusters (20, 22). The underlying clustering mechanism in these cases is unclear.

Here we identified CAPs using a crosslinking agent that only detects proteins up to about 1.5 nm from a target. We provide evidence that most of these CAPs interact with the CCC outside of cadherin clusters. Our results indicate that CCC clusters that integrate CAPs (C-clusters) have fundamentally different structures than the "canonical structures" constrained by cadherin *cis* interactions. We term the latter as "E-clusters" to indicate that

they are driven by extracellular interactions. We found that two CAPs, scribble and erbin, produced a set of CCC clusters that are spatially distinct from E-clusters and from one another. It then appears that C-clusters have distinct properties that depend on those of the CAPs themselves. To establish proof of principle we show that anti-cadherin mAbs, which, similar to CAPs, are too large to be compatible with an E-cluster lattice, generate distinct adhesive clusters. Taken together our data show that CAPs are both able to spatially separate C- from E-clusters and to form CAP-dependent C-clusters that are separate from one another. In addition to their role in cell-cell adhesion, our results thus suggest that CCC clustering serve as a mechanism for organizing cellular proteins into distinct domains within cell-cell contacts.

RESULTS

Most CCC-associated proteins interact with adhesion competent and adhesion-incompetent CCC complexes. Our goal in this section is to determine whether clustering affects the list of CAPs that bind to CCC complexes. To this end we compared the CAPs that associated with functional mGFP-tagged E-cadherin (EcGFP) to those associating with the nonfunctional WK-EcGFP whose two mutations, W2A and K14E, have been shown to completely abolish E-cadherin *trans*-interactions (15, 23). WK-EcGFP was expressed in A431(EP)-ko cells lacking E- and P-cadherins, so as to ensure that P-cadherin adhesive clusters would not recruit the WK mutant through indirect intracellular interactions. To detect even weak, detergent-sensitive interactions, we used an "in cell" crosslinking approach where the cells, before anti-GFP-specific precipitation, were crosslinked using homobifunctional cysteine-specific crosslinker BMPEO3. Due to its short BMPEO3 spacer arm (14.7Å), this approach most likely identifies proteins that directly interact with the CCC. The BioID-based technology, which was used to identify CAP proteins in previous studies (24-26), detects proteins located up to 30 nm away from the target (27). Therefore, the interactome identified in those experiments may reflect the protein composition of the cell cortex and may include proteins that don't interact directly with the CCC. Moreover, previous studies (24) have used low calcium media as a means of generating adhesion-incompetent cadherins. However, this condition produces

atypical *cis* and *trans* cadherin ectodomain interactions, which cannot realistically represent cadherins that don't undergo clustering (28, 29). The use of the WK cadherin mutant ensures that *trans* binding cannot occur and thus provides a more realistic proxy for E-cadherin that is not engaged in cell-cell adhesion.

In agreement with previous studies, the GFP tag in EcGFP did not affect localization of E-cadherin in AJs. Also, as expected, WK-EcGFP was randomly located at the cell surface and unable to form AJs ((15, 23), Fig. 1A, B). After filtering the data through control protein sets obtained from identical pull-down experiment with wild-type A431 cells and with A431(EP)-ko cells expressing a catenin-uncoupled "tailless" E-cadherin mutant EcΔCytoGFP, a list of 59 proteins specifically crosslinked to the cytosolic portion of the CCC was obtained (Fig. 1B, see also SI Appendix, Table S1). Forty-nine of these proteins had been previously detected in association with CCC using BioID (24-26). The most abundant proteins were core CCC members themselves – E- and P-cadherins, α-, β-, p120-catenins and their orthologs present in the majority of epithelial cells, plakoglobin, PKP4, and ARVCF. The remaining 51 proteins could be roughly divided into four functional groups: various adhesion receptors and their adaptors (21 proteins), components of the actin cytoskeleton (11 proteins), different signaling intermediates (12 proteins), and proteins involved in trafficking (2 proteins). Remarkably, the interactomes obtained for EcGFP and WK-EcGFP were nearly identical with respect to both the protein repertoire and spectral counts for individual proteins. Only P-cadherin, that was knocked out in WK-EcGFP-expressing cells, and two low abundant proteins, Septin-9 and CAP1, were undetectable in association with WK-EcGFP (Fig. 1).

Most CAP binding is independent of α-catenin. Three proteins from our list, vinculin, afadin, and VASP, have been shown to be recruited into AJs in response to applied mechanical forces (30-33). Experiments with a molecular tension sensor suggest that CCC outside of adhesive clusters might also be stretched by α-catenin/actin-dependent pooling forces. Such stretching would be relieved upon uncoupling E-cadherin from the actin cytoskeleton by an α-catenin knockout (34). Therefore, we tested the effects of knocking out α-catenin and, surprisingly, while preventing AJ formation (Fig. 1A, B), the knockout removed only 8 proteins from the EcGFP interactome with vinculin, afadin and

VASP remaining bound to the CCC. By contrast, knockout of p120 shortened the list by 22 proteins, including VASP, but did not affect vinculin or afadin. The combined knockout of β-catenin and plakoglobin abolished binding to nearly all proteins with the notable exception of those that interact with juxtamembrane E-cadherin region. Taken together, these data show that the majority of CAPs revealed by our approach interact to a similar extent with both adhesion-competent and adhesion-incompetent CCCs. Furthermore, most of these interactions occur independently of the forces that are generated by the actin cytoskeleton through α-catenin anchorage.

The surprising *trans*-bond-independent presence of vinculin and other force-dependent proteins in our cadherin interactome could in principle be due to the spatial proximity of these proteins in the cell cortex rather than direct physical interactions. To test this scenario, we used Western blotting to analyze BMPEO3-induced adducts containing vinculin or erbin, two CAPs from our list. If these two proteins interact with CCC that spaces their thiols about 15Å apart, BMPEO3 treatment should efficiently generate specific adducts migrating as sharp bands in the SDS-PAGE. If crosslinking is due just to the coalescence of multiple non-interacting proteins, one would expect a smear of accidental adducts. Western blotting of the GFP precipitates obtained from the BMPEO3-treated cells expressing EcGFP and WK-EcGFP confirmed that BMPEO3 generated high amounts of specific vinculin-catenin and erbin-catenin adducts, which were very similar in both cell types (Fig. 2). We also note that the pattern of major BMPEO3 adducts of p120, β-catenin, and α-catenin also showed no significant differences in cells expressing EcGFP or its WK-EcGFP mutant (Fig. 2). These results strongly suggest that, at least, vinculin and erbin form protein complexes with the CCC and their formation is independent of cadherin *trans*-interactions.

CAP-bound clusters segregate from CAP-free CCC clusters. The binding of CAPs to extra-junctional CCC points to the existence of a diverse array of extra-junctional cadherin-catenin supercomplexes (CCSCs), each containing a small number of different CAPs (perhaps only one). Can these CCSCs form distinct C-clusters? Supporting this notion are observations that cell-cell contact localization of vinculin, afadin, LPP, and PS1, in contrast to α- and β-catenins, does not strictly match that of E-cadherin but is

concentrated in specific subregions either within or around CAP-free E-clusters (19, 35-37).

To test whether the sorting of CCSCs into distinct clusters is a common phenomenon, we examined the subcellular localization of two related CAPs from our list, scribble and erbin, both of which had been previously identified in AJs (38-40). No actin-binding activities were noted in these proteins. Immunofluorescence analysis of EcGFP-expressing A431 cells showed that these proteins indeed were localized in AJs but appeared in C-clusters, which overlapped only with a small fraction of the CCC in AJs (Fig. 3A, B and line-scans in C). Inspection of the images and their line-scans showed that well isolated erbin and scribble C-clusters (some are indicated by arrows in Fig. 3C) exhibited much lower EcGFP fluorescence than neighboring E-clusters. To assess the scribble and erbin C-cluster abundance within AJs, we determined a scribble and erbin AJ incorporation index (AJ-II), which we defined as the ratio between the area of erbin- or scribble-specific fluorescence (representing C-clusters) of the selected AJ to the total area of this AJ defined by EcGFP fluorescence, which represents the sum of all C- and E-clusters. The average AJ-II of erbin and scribble was 25% and 10%, respectively, suggesting that the clusters containing either of both proteins represent a relatively small fraction of E-cadherin clusters in AJs (Fig. 3D). Erbin and scribble co-staining showed that their clusters were also distinct from one another (Fig. 3E). Finally, since in some cells erbin is located in desmosomes (41), we verified that in A431 cells, erbin clusters and desmosomes exhibited different distributions (Fig. 3E).

Scribble and erbin clustering depends on E-cadherin trans interactions. To test whether erbin and scribble clustering depend on the E-cadherin *trans* interactions, we studied A431(EP)-ko cells expressing the adhesion incompetent WK-EcGFP mutant. In contrast to observations in EcGFP-expressing A431 cells, in WK-EcGFP cells erbin and scribble as well as the mutant itself did not accumulate in cell-cell contact clusters but were, rather, perinuclear or scattered along the entire plasma membrane (Fig. 3A, B). The loss of erbin and scribble C-clusters was also revealed upon acute disruption of pAJs in EcGFP cells by a function-blocking E-cadherin mAb SHE78-7 (Fig. 3A, B). Altogether these data strongly suggest that the erbin- and scribble-bound CCC forms C-clusters

mediated, at least in part, by E-cadherin *trans* interactions. These two types of C-clusters sort away from one another and from the E-clusters that apparently comprise the bulk of AJs.

There is not enough space for large CAPs within E-clusters. Perhaps the simplest explanation for the sorting of C-clusters from E-clusters is that steric constraints imposed by the 7 nm inter-cadherin spacing in the extracellular lattice preclude the integration of CAPs into the cytoplasmic region of E-clusters. To evaluate this hypothesis, we built molecular models of E-clusters using structural information from X-ray crystallographic and cryo-EM structures wherever possible (Fig. 4 and see SI Appendix, Fig. S1). The model was built by stitching together structures of CCC components reported in the literature (15, 42-48) while connecting them with linkers predicted to be unstructured and, as described in detail in Methods, allowing the maximum possible space between structural regions. We used the 7 nm spacing in the extracellular lattice formed by E-cadherin ectodomains as a constraint for positioning p120, β-catenin, and α-catenin in the model (see details in Methods). The E-cluster was further connected to F-actin via α-catenin ABD domains. The model is almost certainly just a crude representation of an E-cluster but the positions of all proteins in the model with respect to the membrane are in agreement with experimentally determined distances (49-51) and the protein-protein interfaces are taken from experimentally determined structures (15, 43-47). Finally, the membrane is represented schematically in Figure 4 as a box whose width corresponds approximately to the size of E-cadherin's trans-membrane helix (see Methods).

A few details of the model are worth noting. Only small proteins can fit into the lattice, e.g a single PDZ domain is comparable in size to the maximum spacing between β-catenins (see SI Appendix, Fig. S2). Second, we are able to build models that accommodate α-catenin in its folded form, but just barely. Third, since α-catenin is known to partially unfold when binding the E-cadherin/β-catenin complex (52) and vinculin (47), we evaluated whether α-catenin with an unfurled M1 domain (ready to bind vinculin) can form a lattice with vinculin given the distance constraints imposed by cadherins. However, we could not find an arrangement without serious clashes (see Methods for details).

We also assessed whether erbin and scribble would be able to fit into the cytoplasmic region of the E-cluster. These two CAP proteins are composed of LRR and PDZ domains, whose sizes are compared to inter-CCC spacings in Fig. S2 (see SI Appendix). The figure shows two views of CCC complexes in a row along two distinct dimensions of the lattice. The view on the left (see SI Appendix, Fig. S2) has larger spacings between adjacent CCC complexes, and it appears from the figure that there is room for a PDZ domain of erbin or scribble there, but not LRR. We have tried fitting the domains into the lattice, but we found no orientation for LRR domain without clashes (see Methods for details), suggesting that erbin and scribble cannot be accommodated in the E-cluster.

The 67A4 mAb is recruited into AJs through junction reassembly Although the observations reported above involve cytoplasmic proteins, in order to gain mechanistic insights, and as proof of principle, we studied the effects of mAbs that target the E-cadherin ectodomain but do not block cadherin *trans* interactions. We anticipated that such mAbs, given their size, could not be incorporated into the ordered extra-cellular lattice of E-clusters and, in parallel to intracellular CAPs, might form separate clusters. We used mAbs 67A4 and 5H9 that recognize E-cadherin epitopes located on the contiguous EC1 and EC2, and EC2 and EC3 domains, respectively, both of which are outside of the E-cadherin *trans* adhesive interface (53). A standard hanging drop adhesion assay showed that in contrast to the function-blocking SHE78-7 mAb, which completely abolished aggregation of A431 cells, both 67A4 and 5H9 mAbs did not prevent cell aggregation. The resulting cell aggregates exhibited only minor changes; they were more irregular shape in the presence of 67A4 mAb, and they were smaller in size in the presence of 5H9 mAb (see SI Appendix, Fig. S3A). Because all results with these mAbs lead to identical conclusions, only experiments with 67A4 mAb are presented below.

In agreement with the experiments of Petrova et al. (54) with an anti-E-cadherin mAbs with similar properties, 30 min-long incubation of A431 cells at 37ºC with the 67A4 mAb resulted in its incorporation into AJs without any obvious effects on cell morphology (see SI Appendix, Fig. S3B). Furthermore, complete dissolution of the mAb-

labeled AJs after 10 minutes in low calcium media (see SI Appendix, Fig. S3C) verified that the labeled AJs were calcium-dependent and the mAb did not cross-link E-cadherin between neighboring cells. We incubated live and methanol/acetone fixed cells with the mAb at 4º and at 37ºC. Remarkably, in contrast to the fixed cells at both temperatures or live cells at 37ºC, the mAb was completely unable to label AJs in live culture at 4ºC even after 1hr-long incubation (see SI Appendix, Fig. S3D, S3E). This experiment strongly supports the idea that steric constraints impede the direct integration of proteins the size of mAbs, about 15 nm in diameter, into AJs. Continuous remodeling of AJs, including E-cadherin recycling, is apparently needed to deliver mAbs into AJs in living cells.

To fully understand how the mAbs incorporate into the AJs in living cells, we studied the kinetics of this process. The mAb appeared in AJs within 5 min after its addition into the media at 37ºC (see SI Appendix, Fig. S4A, 5 min). After this brief incubation, only small clusters within a subset of AJs became labeled (marked by arrowheads in Fig. S4A and linescan, Fig. S4B, see SI Appendix). The majority of AJs, as in cells stained at 4ºC, exhibited only a weak background fluorescence. With time, the number of the mAb-labeled AJs steadily increased (see SI Appendix, Fig. S4A, 10, 20, and 40 min). Strikingly, instead of gradually accumulating in AJs, the mAb was delivered into the junctions in the form of separate bright clusters typically located at the periphery of the completely unlabeled AJs (see SI Appendix, Fig. S4A, 10 min, and corresponding line-scans Fig. S4B).

Antibody-bound and antibody-free cadherin clusters are incompatible. The experiments described in the previous section show that mAb-bound E-cadherin cannot be intermixed with mAb-free E-cadherin and, rather, forms separate clusters. To further investigate this phenomenon, we incubated the cells with the mAb for 2 min at RT resulting, predominantly, in the labeling of the extra-junctional E-cadherin pool (Fig. 5A, 67A4 2 min). The cells were then chased for additional 30 min in mAb-free media. If able to intermix, mAb-labeled extra-junctional pool and unlabeled junctional E-cadherin pool would eventually produce uniformly labeled AJs. However, we found that the labeled E-cadherin, even after 30 min, formed separate clusters, or very often, just small clusters spatially proximal to the completely unlabeled E-clusters (Fig. 5A, 30 min). To quantify the intermixing of the mAb-labeled and unlabeled E-cadherin, we monitored the Pearson

correlation coefficient (PCC) between the mAb, which marks mAb-bound E-cadherin and β-catenin, which marks total E-cadherin in randomly selected individual AJs. Immediately after pulse labeling, the PCC was about 0.4, and increased over the following 5 min to ~ 0.5 and then remained constant during the following 25 min of observation (Fig. 5B). These results showed that mAb-bound cadherin cannot be intermixed with unlabeled cadherin in AJs despite the fact that the cadherin half-residence time in AJs of A431 cells, as determined by FRAP, is on the order of 2-3 min (55). Instead the labeled E-cadherin forms specific clusters, hereafter "mAb-bound clusters."

mAb-bound E-cadherin cluster formation is mediated by the cadherin trans-binding interface and binding to F-actin. The segregation of mAb-bound and mAb-free E-cadherin clusters suggests that the mAb dramatically changes the cadherin clustering process. One possible explanation is that mAb-bound clusters cannot be dynamically reassembled and thus cannot be intermixed with highly dynamic E-clusters. To determine whether this is the case, EcDn-expressing A431 cells were briefly labeled with the Alexa Fluor 594-labeled 67A4 mAb (0.5 μg/ml) and then imaged in an antibody-free media (Fig. 6A and see also SI Appendix, Movie S1). The obtained movies and superimposition of the subsequent frames showed that the patterns of mAb-bound clusters dramatically changed over the 20 sec-long time window (Fig. 6B). This result shows that the mAb-bound E-cadherin clusters, similar to E-clusters, are continuously and completely reassembled on a sub-minute timescale.

We then tested the role of the E-cadherin strand-swapped *trans* interaction in mAb-bound E-cadherin clustering and found that the mAb did not rescue cadherin clustering in A431EP-ko cells expressing the strand-swap-incompetent W-EcDn mutant (Fig. 6C). In these cells the Alexa Fluor 594-labeled mAb produced only faint fluorescence randomly distributed along the entire surface of the cells (Fig. 6D). This fluorescence, undetected in the control EcDn-expressing A431 cells, was apparently caused by the elevated level of surface E-cadherin that resulted from the inability of the mutant to form AJs.

To test whether mAb-bound cadherin clustering is also α-catenin-dependent, we used α-catenin-depleted A431 cells available in our laboratory (6). Cadherin in these cells, while enriched in some cell-cell contacts, was unable to form AJs (Fig. 6E). Notably, similar to the cells expressing W-EcDn, α-catenin depleted cells failed to form mAb-bound clusters (Fig. 6F). Taken together, these live-imaging experiments showed that mAb-bound clusters are formed through endogenous clustering mechanisms, strand-swapped *trans* dimerization and α-catenin-mediated interaction with actin filaments. Nevertheless, despite these commonalities, mAb-bound clusters sort away from E-clusters.

Discussion

While many of the key protein components of AJs and their interactions have been characterized in atomic detail, the mechanism that coordinates extracellular and intracellular events in cell-cell adhesion is still poorly understood. Although it is clear that the formation of an extracellular paracrystalline cadherin lattice driven by *cis* and *trans* interactions mediates the formation of canonical E-clusters, CCC clustering is still observed for *cis* mutants which ablate the *cis* interaction (20, 22). It may be that in this case the CCC aggregates into amorphous clusters driven by non-specific *cis* interactions on the ectodomain, by *trans*-membrane helical interactions, and/or by other CCC components. Independent of detailed mechanism, the formation of cadherin clusters under conditions where ordered *cis*-interaction driven ectodomain lattices cannot be formed suggests that additional clustering mechanisms play a role in AJ structure and dynamics. Here we have shown that CCC-associated proteins (CAPs) can facilitate clustering and that the properties of the resulting clusters are dependent on the nature of individual CAPs.

How are CAPs integrated into CCC clusters? In Fig. 4 we have built a crude model of a E-cluster constrained by a 70Å distance between cadherin tails emerging from the membrane as defined by the ectodomain lattice. It seems clear from the model that the

binding of many CAP proteins to the CCC is incompatible with a cadherin lattice so that direct integration into E-clusters is highly unlikely. For example, there is no room for vinculin in E-clusters so that its binding to α-catenin could only occur outside the paracrystaline cadherin lattice. Moreover, separate C-clusters, which incorporate vinculin, or other CAPs must be organized in a very different way than lattice-driven E-clusters.

Our data suggest that CAPs interact with the extra-junctional CCCs forming CCC supercomplexes, which then assemble into C-clusters. Supporting this model is our comparison of the interactomes of functional E-cadherin, EcGFP, with that of the adhesion incompetent E-cadherin mutant, WK-EcGFP, which is unable to undergo *trans* interactions (23, 56). Strikingly, the list of proteins associated with WK-EcGFP is nearly identical to that associated with EcGFP. Taken together our data clearly indicate that junctional C-clusters are formed, not through selective binding of a particular CAP to an E-cluster, but through the self-assembly of preformed CCC-CAP supercomplexes (CCSCs).

Of note, the list of CAPs is shortened by only 8 proteins in α-catenin knockout cells. Interestingly, vinculin, afadin and VASP, which were shown to interact with the CCC through α-catenin in a tension-dependent manner (31, 46) bind to the CCC even in the knockout. By contrast, the list of CAPs is shortened by 20 proteins in p120 deficient cells, despite the fact that these cells retain AJs. Combined β-catenin/plakoglobin knockout results even in more dramatic reduction in the list of CAPs, suggesting that these two proteins provide binding sites for most of the CAPs. Since, as we argue in Fig. 4, there is no room for most CAPs within E-clusters, we are led to the conclusion that most CAPs interact with β-catenin and/or p120 in extra-junctional space and then form distinct C-clusters. Consistent with our results, vinculin was shown to interact with the CCC even in the absence of α-catenin (57-59). Taken together the available data thus suggests that a vinculin-CCC supercomplex delivers vinculin to the sites of cell-cell adhesion, where vinculin binds to α-catenin in a process related in a still undefined way with C-cluster formation. The latter process is apparently force-dependent. Of note, both force-independent and force-dependent steps have recently been shown to participate in the recruitment of vinculin into Focal Adhesions (60).

To probe the formation of C-clusters with CAPs that are not known to interact with actin, we studied the localization of erbin and scribble, that we identified in the CCC interactome. They have both been previously detected in AJs (38-40, 61) and do not possess known actin-binding domains. Immunofluorescence microscopy confirmed previous observations that scribble and erbin are localized in AJs. However, we show here that the distribution of these proteins in AJs is not uniform. In fact, they both are integrated into only a subset of C-clusters that are either proximal to or surrounded by other types of C-clusters, or by E-clusters, which comprise the bulk of AJs. Moreover, the C-clusters incorporating erbin and scribble do not overlap with one another. The existence of both, erbin- and scribble-specific clusters clearly depends on cadherin adhesive interactions since they are lost in cells expressing adhesion-incompetent WK-EcGFP mutant or immediately disassemble after administration of the function-blocking E-cadherin mAb.

Taken together our results suggest that CAPs associate with extra-junctional CCC and only then, in form of the cadherin-catenin supercomplexes (CCSCs), assemble C-clusters that are spatially and structurally distinct from E-clusters. At this stage we have no direct evidence as to how CCC-clusters assemble but we speculate that assembly is facilitated by CAP-specific *cis* interactions thus providing a mechanism for the formation of individual clusters. For example, two of the four PDZ domains of scribble interact with β-catenin and another one interacts with p120 orthologs, δ-catenin, PKP4, and ARVCF (62). It is possible that these interactions play a role in the assembly of scribble-specific clusters. Similarly, dimerization of vinculin upon binding to F-actin might also play a "CCC-organizing" role (63).

As proof of principle, we studied two E-cadherin mAbs, 67A4 and 5H9, which abolish cadherin *cis* interactions but leave the *trans*-binding interface unaltered (53). Our results show that the mAbs are unable to interact with E-cadherin in AJs, but, rather bind to extra-junctional E-cadherin. Furthermore, instead of being intermixed with the mAb-free E-cadherin in AJs, the mAb-bound E-cadherin generates separate adhesion clusters. Under conditions of mAb excess, the mAb-bound clusters dominate and eventually replace the mAb-free AJs. When mAb-bound and mAb-free E-cadherin pools coexist, the cells continue to exhibit two pools of clusters. The data show that both, the mAb-bound

and mAb-free E-cadherin still use *trans* interactions and α-catenin binding to F-actin for their clustering. Importantly, the mAbs, which are applied from outside, preclude any possibility that the observed segregation of mAb-bound and mAb-free E-cadherin clusters occurs as a result of antibody-mediated binding of the CCC to any specific intracellular structures. While the mAb experiments involve extracellular phenomena and our focus in this work is on CAPs that associate with the cytosolic portion of CCC, the experiments with mAbs demonstrate the possibility of coexistence of different types of CCC clusters all of which are based on the same cadherin *trans* interactions.

In conclusion, we present strong evidence that at least some CAPs cannot be integrated into E-clusters, but form CAP-specific C-clusters. We speculate that formation of these C-clusters is driven by *cis* interactions provided by the CAPs themselves, that play a similar role as cadherin *cis* interactions in E-clusters. An important consequence of this model is that the structural organization of CAP-specific clusters must be matched on two sides of an adhesion interface. Such complementarity in composition would ultimately equalize the number of C-clusters containing particular CAPs in neighboring cells. The structural synergism between *trans*- and *cis*-interactions that has been shown to play a role in adhesion (8, 64), could function, therefore, as sorting mechanism that arranges CAPs – various receptors, signaling intermediates and their adaptors – into specialized clusters that are equivalent in structure and number to those in neighboring cells. This feature of cadherin-based adhesion might potentially synchronize signaling events in individual cells in a given tissue.

Materials and Methods

Plasmids. The plasmids encoding Ec-mGFP (denoted EcGFP), EcΔCytoGFP, Ec-Dn have been reported (7, 17). Mutations W2A inserted into Ec-Dn (W-EcDn) and W2A/K14E inserted into Ec-mGFP (WK-EcGFP) were described by Hong et al. (23). mCherry-tagged E-cadherin, EcCH, was constructed from pRc-EcDn by replacing the tags. The plasmid pRcCMV-P1EcDn was constructed by the replacement of the N-terminal region of E-cadherin in EcDn with the homological region of P1Ec-Myc (65). All plasmid inserts were verified by sequencing.

Cell culture, transfection, and cell labeling. The cells, A431D, A431, A431-EcDn, α-catenin deficient A431 cells (A431aCat-sh) had been previously described (6, 19, 66). Ec-mGFP (EcGFP-) and W-EcDn-expressing A431E-ko cells were obtained using stable transfection with the corresponding plasmids of the A431E-ko cells in which endogenous E-cadherin was knocked out using Alt-R CRISPR-Cas9 System (IDT) (7). The catenin-knockout cells were obtained using the same protocol. In brief, the EcGFP-A431E-ko cells were transfected with an RNA complex consisting of a gene-specific CRISPR RNA (crRNA; designed by software of Broad Institute of Harvard and Massachusetts Institute of Technology) and transactivating RNA (tracrRNA). The following crRNAs were used: p120-5'-GTGAAGCTCGCCGGAAACTT; β-catenin -5'-GAAACAGCTCGTTGTACCGC; plakoglobin-5'- CATGGCCTCCCGCACCCGTT; α-catenin-5'- GAAGGGGGATAAAATTGCGA. Similarly, WK-EcGFP cells were obtained after transfection of the A431(EP)-ko cells in which both E- and P-cadherin were silenced using the same approach. The hanging drop assay was performed as described by Kim et al. (67). In brief, about $1.5x10^5$ cells in 30 ml were seeded onto the inner surface of a 35-mm culture dishes as hanging drops and allowed to aggregate overnight. To assay for tightness of cell–cell adhesion, the drops were passed 10 times through a standard 200-μl pipet tip. The resulting suspension was imaged through a 10x phase-contrast objective.

For mAb-binding experiments, the 67A4 (Millipore, MAB-3199Z), 5H9 (Santa Cruz, sc-52327), or SHE78-7 (Zymed Laboratories, South San Francisco, CA) mAbs (azid-free) were added into the culture media at final concentration 2 μg/ml and incubated as indicated. For live-cell imaging the cells were labeled by adding into the cultures the Alexa Fluor 594-conjugated 67A4 mAb (Azide free; BioLegend Inc, San Diego, CA) at final concentration 1.2 μg/ml for 2 min. The cells were incubated for 1-2 min in the labeling media and, after brief washing, the labeled cells were imaged in the label-free imaging media.

Immunofluorescence microscopy. For immunofluorescence, cells were fixed and permeabilized with 3% formaldehyde-1% Triton X-100. See a study by Indra et al. for details (19). Wide-field images were taken using Eclipse 80i Nikon microscope (Plan Apo 100×/1.40 objective lens) and a digital camera (CoolSNAP EZ; Photometrics,

Tucson, AZ). The images were then processed using Nikon's NIS-Elements software. For immunostaining the following antibodies were used: mouse mAb anti-E-cadherin clone HECD1 (Zymed Laboratories) and anti-p120 (BD Trunsduction Laboratories); sheep anti-erbin (R&D biosystem, AF7866), rabbit anti-Dendra2 (Evrogen, Moscow, Russia); anti-β-catenin and anti-PLEKHA5 (Invitrogen, MA5-14461 and PA5-57463); anti-myosin 1c, anti-scribble, anti-α-catenin (Abcam, ab194828, ab36708, and ab51032). All secondary antibodies were produced in Donkey (Jackson Immunoresearch Laboratories).

Live-cell imaging and data processing. The experiments were performed essentially as described earlier (17, 55) using halogen (Figs 4, 5, 7A, 9C) and mercury (Figs 7B, 8) light sources. In brief, cells were imaged (in L-15 media with 10% FBS) by Eclipse Ti-E microscope (Nikon, Melville, NY) at 37ºC controlled with Nikon's NIS-Elements software. The microscope was equipped with an incubator chamber, a CoolSNAP HQ2 camera (Photometrics) and a Plan Apo VC 100x/1.40 lens. The 2x2 binning mode was used in all live-imaging experiments. At this microscope setting the pixel size was 128 nm. All images were saved as Tiff files and processed using ImageJ software (National Institutes of Health).

For standard line scan analysis Fiji (NIH) plot profile tool was used. Briefly, one pixel width line was drawn along the selected contact on the merged images. The line was restored accurately on the green and red images separately using “Restore previous selection” command. Individual plots were then created using “Plot profile” command for red and green images. The final graphs were created with Microsoft excel with the calculated plot values. AJ-II determination was performed using Fiji (NIH). For each protein staining, 14 individual pAJs of 25-50 pixels in length, were cropped using manual cropping tool. The fraction of these pAJs occupying by red fluorescence was calculated by using color threshold tool by measuring total green area and red area within the green area. The standard error was calculated and plotted accordingly.

Proteomics. The confluent cultures of indicated cells grown on 10 cm plates were crosslinked using BMPEO3 crosslinker as we described previously (66), then lysed with the Lysis Buffer (LB, 20 mM TrisHCl, 150 mM NaCl, 2 mM EDTA, and 1% Triton X-100) and cleared by centrifugation and incubated for 1 h with 30 μl of GFP-trap beads (Chromotek). After incubation, the beats were washed 4 times in LB, boiled in 30 ml of

SDS-sample buffer and load on SDS-PAAG. The samples were run through 4-12% SDS-PAAGE and the samples were submitted to the Proteomics facility of the Northwestern University where they were subjected to in-gel reduction, alkylation, tryptic digestion and subsequent quantitative MS analyses.

Raw quantitative MS/MS data was obtained via Scaffold Viewer's (Version: Scaffold_4.9.0) complete export function. Total spectra counts were automatically normalized through Scaffold's algorithm, where UniProt database (the uniprot-SP-human_20180326_20190417 database (unknown version, 20303 entries) was applied for the purpose of identification. Protein identification threshold was set to 1% false discovery rate.

A total of 7 samples independently obtained from EcGFP-A431E-ko cells were quantified. Using R Studio (Version: 3.6.0 (2019-04-26)), each sample columns were joined by their respective unique ID (gene name) to reproduce a merged data frame. Proteins with less than or equal to 4 identifications across all 7 samples were excluded from further data processing. Mean spectra counts were then calculated for the remaining proteins. Similar technique described above was applied to obtain maximum spectra count values for the samples obtained from A431 cells (11 samples) and mean spectra counts for the samples obtained from A431E-ko cells expressing EcΔCytoGFP (6 samples). These values were then applied against mean values of E-cadherin to identify contaminants and non-specific proteins. In both combinations, proteins with spectra counts greater than 20% of E-cadherin mean were subject to removal, with the exception of CDH1 and CDH3. A total of 59 proteins remained. Using the spectra counts of E-cadherin sample set as a source, two-tailed t-test was applied to the remaining 61 proteins to observe individual p values (at $\alpha = 0.05$). The same procedure was used for analyses from 3 to 5 samples of EcGFP-A431Ec-ko cells with additional knocked out α-catenin, p120 and combination of plakoglobin and β-catenin. For Western blot analysis, the GFP-trap precipitates together with a sample of protein markers (10-450 kDa, Invitrogen) were separated on 3-8% Tris-acetate gels (Invitrogen) and transferred to nitrocellulose membrane (Millipore). Cell Surface Proteins were biotinylated exactly as described (36). In brief, the confluent cultures (grown on 6-cm dishes) were washed and incubated at 4°C

with 2 ml of 0.5 mg/ml sulfo-NHC-LC-biotin (Pierce Chemical) in PBS-Ca for 5 min. The cell lysates were obtained using LB (see above) and biotinylated protein were then precipitated by streptavidin agarose and analyzed by immunoblotting.

Structural modeling E-clusters bound to actin. The extracellular E-cadherin lattice was built using the "generate symmetry mates" option in the PyMOL Molecular Graphics System, Version 2.2.0, Schrodinger LLC as applied to a crystal structure of E-cadherin featuring both trans- and cis- interactions among ectodomains (PDBID: 3Q2V, (15)). Cα atoms at the C-terminal of EC5 domains of E-cadherins in a 3x3 lattice were used as guides for constraints when placing cytoplasmic components into the lattice with every protein structure translated according to distances and angles shown in Fig. S1 (see SI Appendix). The following crystal structures were used (PDBIDs given in parenthesis) when combining fragments of cytoplasmic components together: p120 bound to E-cadherin (3L6X, (44)), β-catenin bound to E-cadherin (1I7W, 1I7X, (43)), head domain of α-catenin bound to β-catenin (4ONS, chains C and D, (46)), full length α-catenin (4IGG, (48)), full-length vinculin (1TR2, (42)), and human vinculin head domain in complex with unfurled M-domain fragment of α-catenin (4EHP, (47)).

All structures were stitched together either by structural superposition (whenever structures had overlapping regions) or by building linkers to connect the fragments in unstructured regions. The following C-terminal sequence stretches were modelled as linkers in PyMOL: 691-705, 732-755, 774-781, 839-851. The transmembrane (TM) portion of E-cadherin, 707-731, predicted based on its helical secondary structure and high positive TMpred scores (https://embnet.vital-it.ch/software/TMPRED_form.html), was modeled as a single pass helix in Coot (Version 0.8.9.1, (68)). The helix is about ~33Å in length, flanked by unstructured polar (Gln) or charged (Arg) residues, and oriented perpendicular to the plane of the membrane in Figure 4. The residue numbers correspond to the human E-cadherin sequence (Uniprot ID P12830). Geometry of all modelled regions was further regularized in Coot.

Arrangement of p120 with respect to β-catenin. A short E-cadherin linker of 8 amino acids connects the two complexes. The linker ends are located near the N-terminal of p120 and the middle of the β-catenin armadillo repeat domain thus placing p120 and β-

catenin in close proximity (it is also evident from the presented cross-linking experiment, see Fig. 2), but whether an interface is formed between the two is unknown. We built a p120/β-catenin complex by docking the p120/E-cadherin heterodimer against the β-catenin/E-cadherin complex using ClusPro (69) and picking a top scoring model that would satisfy two conditions: 1) orientation between p120 and β-catenin would be compatible with an eight amino acid long linker between E-cadherin tails that were structurally unresolved; 2) the orientation should be as extended as possible to provide maximum space between the lattice components.

Incorporating α-catenin into the lattice. It was difficult to find orientations of CCC components that would allow folded α-catenin to exist in the lattice without steric clashes. SAXS data (52) suggests that when α-catenin binds E-cadherin/β-catenin structural rearrangement occurs leading to separation of the head and M domain. However, we did not consider this possibility in our modeling due to the lack of available coordinates of the E-cadherin/β-catenin/α-catenin complex. Thus, the folded form of α-catenin was used in our modeling.

To find orientations that might allow α-catenin to fit into the lattice without clashes we created 1728 2x2 lattices of full-length α-catenin/β-catenin heterodimers that are compatible with extracellular E-cadherin spacing. Rigid heterodimers were rotated by different combinations of roll, pitch, yaw Euler angles (from α,β,γ=0° to α,β,γ=330° with step of 30°) and then translated into the 2x2 lattice (see SI Appendix, Fig. S5A). Each orientation was then evaluated for clashes by counting the number of atoms that are in close proximity to one other between distinct heterodimers in the lattice. All lattice configurations had clashes defined by a 4Å distance cutoff between atoms, approximately the sum of the effective van der Waals radius of CH2 groups (see SI Appendix, Fig. S5B). A model with a minimal number of 4 such clashing atoms (see SI Appendix, Fig. S5C), was chosen to represent the orientation of α-catenin/β-catenin in the lattice.

Incorporating vinculin into the lattice. We first built a model of an α-catenin/vinculin complex (see SI Appendix, Fig. S6A). In this model, the M1 domain of α-catenin is unfolded – in agreement with the crystal structure of the complex containing protein fragments (47), top left panel in Fig. S6A, see SI Appendix), while the head and M-

domain of α-catenin no longer share an interface (in agreement with SAXS data (52)). Using the same approach as discussed in the paragraph above (see SI Appendix, Fig. S5A) we generated 1728 2x2 lattices using an α-catenin/vinculin heterodimer shown in Fig. S5B, see SI Appendix. All lattice configurations resulted in severe clashes (see SI Appendix, Fig. S6C). We then built a more compact model of α-catenin/vinculin (see SI Appendix, Fig. S6D) where the M-domain of α-catenin was reoriented with respect the original model (see SI Appendix, Fig. S6B) so as to allow the fewest possible clashes as determined by visual inspection. However, extended sampling still failed to produce a clash-free structure (see SI Appendix, Fig. S6E). We note that all α-catenin/vinculin heterodimers we considered lacked ABD domains. These domains have previously been shown (44, 52, 70-73) to be easily detachable from the rest of the protein so as to bind actin (see SI Appendix, Fig. S7).

Incorporating erbin and scribble into the lattice. Erbin has a leucine-rich repeat (LRR) domain followed by a PDZ domain. Scribble has a LRR domain followed by four PDZ domains comparable in size to those of erbin. Fig. S2 (see SI Appendix) compares the size of PDZ and LRR domains to spacings in the lattice. We show a representative PDZ domain of scribble (PDBID 5VWC, orange (74)) and a top structural template (E-value < 10^{-28} in HHPRED search (75)) found for LRR domains of both scribble and erbin sequences (PDBID 4U09, yellow (76)); structures of LRR domains of scribble and erbin have not been solved yet. The view of Fig. S2 (see SI Appendix) was chosen to show the maximum distance available between CCC complexes along two distinct dimensions in the lattice, and by visual observation PDZ domain can barely fit into the maximum spacing while LRR cannot. We also tried fitting these two domains manually into the lattice using PyMOL and we were unable to find orientations with no clashes for the LRR domain. Moreover, if p120 and β-catenin were not to form an interface (as modelled in the lattice) and instead assumed a more distant orientation with respect to one another, there would be even no space for a PDZ domain of erbin and scribble in the E-cluster, as it barely fits between CCC complexes of the current model.

Attachment to actin. An actin filament decorated by ABDs (Fig. 4) was built by combining three identical cryo-EM structures of the F-actin/ABD complex (PDBID: 6UPV, (45)) via superimposition of G-actins in PyMOL. F-actin/ABD was oriented

manually in PyMOL to be parallel and equidistant from two CCC rows of the 3x3 lattice. α-catenin ABD domains in these two CCC rows were then removed and the M-domains of folded α-catenins were attached to ABDs on F-actin via flexible linkers modelled in Coot (these linkers, longer than 60 amino acids, have no crystal structure available).

Acknowledgments

We thank Drs. B. Mitchell for valuable discussions and suggestions. Proteomics, Sequencing and Flow Cytometry were performed at the Northwestern University Proteomics Center of Excellence, Genetic. and Flow Cytometry Facilities. The authors declare no competing financial interests. The work was supported by grants from the National Institutes of Health: AR44016 and AR057992 (S.T.), NSF grant MCB-1914542 (B.H.) and NIH grants R01GM118584 and R01MH114817 to (L.S.).

References

1. K. J. Green, S. Getsios, S. Troyanovsky, L. M. Godsel, Intercellular junction assembly, dynamics, and homeostasis. *Cold Spring Harb Perspect Biol* **2**, a000125 (2010).
2. B. M. Gumbiner, Regulation of cadherin-mediated adhesion in morphogenesis. *Nat Rev Mol Cell Biol* **6**, 622-634 (2005).
3. T. J. Harris, U. Tepass, Adherens junctions: from molecules to morphogenesis. *Nat Rev Mol Cell Biol* **11**, 502-514 (2010).
4. C. M. Niessen, D. Leckband, A. S. Yap, Tissue organization by cadherin adhesion molecules: dynamic molecular and cellular mechanisms of morphogenetic regulation. *Physiol Rev* **91**, 691-731 (2011).
5. C. D. Buckley *et al.*, Cell adhesion. The minimal cadherin-catenin complex binds to actin filaments under force. *Science* **346**, 1254211 (2014).
6. C. S. Chen *et al.*, alpha-Catenin-mediated cadherin clustering couples cadherin and actin dynamics. *J Cell Biol* **210**, 647-661 (2015).
7. I. Indra *et al.*, Spatial and temporal organization of cadherin in punctate adherens junctions. *Proc Natl Acad Sci U S A* **115**, E4406-E4415 (2018).
8. Y. Wu, J. Vendome, L. Shapiro, A. Ben-Shaul, B. Honig, Transforming binding affinities from three dimensions to two with application to cadherin clustering. *Nature* **475**, 510-513 (2011).

9. J. Brasch, O. J. Harrison, B. Honig, L. Shapiro, Thinking outside the cell: how cadherins drive adhesion. *Trends Cell Biol* **22**, 299-310 (2012).
10. R. M. Mege, N. Ishiyama, Integration of Cadherin Adhesion and Cytoskeleton at Adherens Junctions. *Cold Spring Harb Perspect Biol* **9** (2017).
11. S. Troyanovsky, Adherens junction assembly. *Subcell Biochem* **60**, 89-108 (2012).
12. A. S. Yap, G. A. Gomez, R. G. Parton, Adherens Junctions Revisualized: Organizing Cadherins as Nanoassemblies. *Dev Cell* **35**, 12-20 (2015).
13. I. Indra, R. B. Troyanovsky, L. Shapiro, B. Honig, S. M. Troyanovsky, Sensing Actin Dynamics through Adherens Junctions. *Cell Rep* **30**, 2820-2833 e2823 (2020).
14. A. S. Yap, W. M. Brieher, M. Pruschy, B. M. Gumbiner, Lateral clustering of the adhesive ectodomain: a fundamental determinant of cadherin function. *Curr Biol* **7**, 308-315 (1997).
15. O. J. Harrison *et al.*, The extracellular architecture of adherens junctions revealed by crystal structures of type I cadherins. *Structure* **19**, 244-256 (2011).
16. S. D. Hansen *et al.*, alphaE-catenin actin-binding domain alters actin filament conformation and regulates binding of nucleation and disassembly factors. *Mol Biol Cell* **24**, 3710-3720 (2013).
17. S. Hong, R. B. Troyanovsky, S. M. Troyanovsky, Binding to F-actin guides cadherin cluster assembly, stability, and movement. *J Cell Biol* **201**, 131-143 (2013).
18. X. P. Xu *et al.*, Structural basis of alphaE-catenin-F-actin catch bond behavior. *Elife* **9** (2020).
19. I. Indra, S. Hong, R. Troyanovsky, B. Kormos, S. Troyanovsky, The adherens junction: a mosaic of cadherin and nectin clusters bundled by actin filaments. *J Invest Dermatol* **133**, 2546-2554 (2013).
20. P. O. Strale *et al.*, The formation of ordered nanoclusters controls cadherin anchoring to actin and cell-cell contact fluidity. *J Cell Biol* **210**, 1033 (2015).
21. B. A. Truong Quang, M. Mani, O. Markova, T. Lecuit, P. F. Lenne, Principles of E-cadherin supramolecular organization in vivo. *Curr Biol* **23**, 2197-2207 (2013).
22. R. B. Troyanovsky, I. Indra, C. S. Chen, S. Hong, S. M. Troyanovsky, Cadherin controls nectin recruitment into adherens junctions by remodeling the actin cytoskeleton. *J Cell Sci* **128**, 140-149 (2015).
23. S. Hong, R. B. Troyanovsky, S. M. Troyanovsky, Cadherin exits the junction by switching its adhesive bond. *J Cell Biol* **192**, 1073-1083 (2011).
24. Z. Guo *et al.*, E-cadherin interactome complexity and robustness resolved by quantitative proteomics. *Sci Signal* **7**, rs7 (2014).
25. Y. Li *et al.*, The N-cadherin interactome in primary cardiomyocytes as defined using quantitative proximity proteomics. *J Cell Sci* **132** (2019).
26. C. M. Van Itallie *et al.*, Biotin ligase tagging identifies proteins proximal to E-cadherin, including lipoma preferred partner, a regulator of epithelial cell-cell and cell-substrate adhesion. *J Cell Sci* **127**, 885-895 (2014).
27. K. J. Roux, D. I. Kim, M. Raida, B. Burke, A promiscuous biotin ligase fusion protein identifies proximal and interacting proteins in mammalian cells. *J Cell Biol* **196**, 801-810 (2012).

28. R. B. Troyanovsky, J. Klingelhofer, S. Troyanovsky, Removal of calcium ions triggers a novel type of intercadherin interaction. *J Cell Sci* **112 (Pt 23)**, 4379-4387 (1999).
29. R. B. Troyanovsky, E. Sokolov, S. M. Troyanovsky, Adhesive and lateral E-cadherin dimers are mediated by the same interface. *Mol Cell Biol* **23**, 7965-7972 (2003).
30. Q. le Duc *et al.*, Vinculin potentiates E-cadherin mechanosensing and is recruited to actin-anchored sites within adherens junctions in a myosin II-dependent manner. *J Cell Biol* **189**, 1107-1115 (2010).
31. J. M. Leerberg *et al.*, Tension-sensitive actin assembly supports contractility at the epithelial zonula adherens. *Curr Biol* **24**, 1689-1699 (2014).
32. K. Matsuzawa, T. Himoto, Y. Mochizuki, J. Ikenouchi, alpha-Catenin Controls the Anisotropy of Force Distribution at Cell-Cell Junctions during Collective Cell Migration. *Cell Rep* **23**, 3447-3456 (2018).
33. S. Yonemura, Y. Wada, T. Watanabe, A. Nagafuchi, M. Shibata, alpha-Catenin as a tension transducer that induces adherens junction development. *Nat Cell Biol* **12**, 533-542 (2010).
34. N. Borghi *et al.*, E-cadherin is under constitutive actomyosin-generated tension that is increased at cell-cell contacts upon externally applied stretch. *Proc Natl Acad Sci U S A* **109**, 12568-12573 (2012).
35. I. Indra, R. Troyanovsky, S. M. Troyanovsky, Afadin controls cadherin cluster stability using clathrin-independent mechanism. *Tissue Barriers* **2**, e28687 (2014).
36. A. Kiss, R. B. Troyanovsky, S. M. Troyanovsky, p120-catenin is a key component of the cadherin-gamma-secretase supercomplex. *Mol Biol Cell* **19**, 4042-4050 (2008).
37. J. Oldenburg *et al.*, VASP, zyxin and TES are tension-dependent members of Focal Adherens Junctions independent of the alpha-catenin-vinculin module. *Sci Rep* **5**, 17225 (2015).
38. J. Choi, R. B. Troyanovsky, I. Indra, B. J. Mitchell, S. M. Troyanovsky, Scribble, Erbin, and Lano redundantly regulate epithelial polarity and apical adhesion complex. *J Cell Biol* **218**, 2277-2293 (2019).
39. R. P. Laura *et al.*, The Erbin PDZ domain binds with high affinity and specificity to the carboxyl termini of delta-catenin and ARVCF. *J Biol Chem* **277**, 12906-12914 (2002).
40. C. Navarro *et al.*, Junctional recruitment of mammalian Scribble relies on E-cadherin engagement. *Oncogene* **24**, 4330-4339 (2005).
41. R. M. Harmon *et al.*, Desmoglein-1/Erbin interaction suppresses ERK activation to support epidermal differentiation. *J Clin Invest* **123**, 1556-1570 (2013).
42. R. A. Borgon, C. Vonrhein, G. Bricogne, P. R. Bois, T. Izard, Crystal structure of human vinculin. *Structure* **12**, 1189-1197 (2004).
43. A. H. Huber, W. I. Weis, The structure of the beta-catenin/E-cadherin complex and the molecular basis of diverse ligand recognition by beta-catenin. *Cell* **105**, 391-402 (2001).
44. N. Ishiyama *et al.*, Dynamic and static interactions between p120 catenin and E-cadherin regulate the stability of cell-cell adhesion. *Cell* **141**, 117-128 (2010).

45. L. Mei *et al.*, Molecular mechanism for direct actin force-sensing by alpha-catenin. *Elife* **9** (2020).
46. S. Pokutta, F. Drees, Y. Takai, W. J. Nelson, W. I. Weis, Biochemical and structural definition of the l-afadin- and actin-binding sites of alpha-catenin. *J Biol Chem* **277**, 18868-18874 (2002).
47. E. S. Rangarajan, T. Izard, The cytoskeletal protein alpha-catenin unfurls upon binding to vinculin. *J Biol Chem* **287**, 18492-18499 (2012).
48. E. S. Rangarajan, T. Izard, Dimer asymmetry defines alpha-catenin interactions. *Nat Struct Mol Biol* **20**, 188-193 (2013).
49. C. Bertocchi *et al.*, Nanoscale architecture of cadherin-based cell adhesions. *Nat Cell Biol* **19**, 28-37 (2017).
50. M. G. Farquhar, G. E. Palade, Junctional complexes in various epithelia. *J Cell Biol* **17**, 375-412 (1963).
51. N. S. McNutt, R. S. Weinstein, Membrane ultrastructure at mammalian intercellular junctions. *Prog Biophys Mol Biol* **26**, 45-101 (1973).
52. M. Bush *et al.*, An ensemble of flexible conformations underlies mechanotransduction by the cadherin-catenin adhesion complex. *Proc Natl Acad Sci U S A* **116**, 21545-21555 (2019).
53. O. Y. Laur, J. Klingelhofer, R. B. Troyanovsky, S. M. Troyanovsky, Both the dimerization and immunochemical properties of E-cadherin EC1 domain depend on Trp(156) residue. *Arch Biochem Biophys* **400**, 141-147 (2002).
54. Y. I. Petrova, M. M. Spano, B. M. Gumbiner, Conformational epitopes at cadherin calcium-binding sites and p120-catenin phosphorylation regulate cell adhesion. *Mol Biol Cell* **23**, 2092-2108 (2012).
55. S. Hong, R. B. Troyanovsky, S. M. Troyanovsky, Spontaneous assembly and active disassembly balance adherens junction homeostasis. *Proc Natl Acad Sci U S A* **107**, 3528-3533 (2010).
56. O. J. Harrison *et al.*, Two-step adhesive binding by classical cadherins. *Nat Struct Mol Biol* **17**, 348-357 (2010).
57. R. B. Hazan, L. Kang, S. Roe, P. I. Borgen, D. L. Rimm, Vinculin is associated with the E-cadherin adhesion complex. *J Biol Chem* **272**, 32448-32453 (1997).
58. X. Peng, J. L. Maiers, D. Choudhury, S. W. Craig, K. A. DeMali, alpha-Catenin uses a novel mechanism to activate vinculin. *J Biol Chem* **287**, 7728-7737 (2012).
59. S. Ray, H. P. Foote, T. Lechler, beta-Catenin protects the epidermis from mechanical stresses. *J Cell Biol* **202**, 45-52 (2013).
60. S. J. Han *et al.*, Pre-complexation of talin and vinculin without tension is required for efficient nascent adhesion maturation. *Elife* **10** (2021).
61. Y. Sun, M. Aiga, E. Yoshida, P. O. Humbert, S. X. Bamji, Scribble interacts with beta-catenin to localize synaptic vesicles to synapses. *Mol Biol Cell* **20**, 3390-3400 (2009).
62. T. T. Bonello, M. Peifer, Scribble: A master scaffold in polarity, adhesion, synaptogenesis, and proliferation. *J Cell Biol* **218**, 742-756 (2019).
63. C. E. Tolbert, P. M. Thompson, R. Superfine, K. Burridge, S. L. Campbell, Phosphorylation at Y1065 in vinculin mediates actin bundling, cell spreading, and mechanical responses to force. *Biochemistry* **53**, 5526-5536 (2014).

64. Y. Wu *et al.*, Cooperativity between trans and cis interactions in cadherin-mediated junction formation. *Proc Natl Acad Sci U S A* **107**, 17592-17597 (2010).
65. J. Klingelhofer, R. B. Troyanovsky, O. Y. Laur, S. Troyanovsky, Amino-terminal domain of classic cadherins determines the specificity of the adhesive interactions. *J Cell Sci* **113 (Pt 16)**, 2829-2836 (2000).
66. R. B. Troyanovsky, J. Klingelhofer, S. M. Troyanovsky, alpha-Catenin contributes to the strength of E-cadherin-p120 interactions. *Mol Biol Cell* **22**, 4247-4255 (2011).
67. J. B. Kim *et al.*, N-Cadherin extracellular repeat 4 mediates epithelial to mesenchymal transition and increased motility. *J Cell Biol* **151**, 1193-1206 (2000).
68. P. Emsley, B. Lohkamp, W. G. Scott, K. Cowtan, Features and development of Coot. *Acta Crystallogr D Biol Crystallogr* **66**, 486-501 (2010).
69. D. Kozakov *et al.*, The ClusPro web server for protein-protein docking. *Nat Protoc* **12**, 255-278 (2017).
70. N. Ishiyama *et al.*, An autoinhibited structure of alpha-catenin and its implications for vinculin recruitment to adherens junctions. *J Biol Chem* **288**, 15913-15925 (2013).
71. M. E. Janssen *et al.*, Three-dimensional structure of vinculin bound to actin filaments. *Mol Cell* **21**, 271-281 (2006).
72. B. M. Jockusch, M. Rudiger, Crosstalk between cell adhesion molecules: vinculin as a paradigm for regulation by conformation. *Trends Cell Biol* **6**, 311-315 (1996).
73. I. D. Nicholl *et al.*, alpha-Catenin Structure and Nanoscale Dynamics in Solution and in Complex with F-Actin. *Biophys J* **115**, 642-654 (2018).
74. K. Y. B. Lim, N. J. Godde, P. O. Humbert, M. Kvansakul, Structural basis for the differential interaction of Scribble PDZ domains with the guanine nucleotide exchange factor beta-PIX. *J Biol Chem* **292**, 20425-20436 (2017).
75. L. Zimmermann *et al.*, A Completely Reimplemented MPI Bioinformatics Toolkit with a New HHpred Server at its Core. *J Mol Biol* **430**, 2237-2243 (2018).
76. P. J. Collins *et al.*, Recent evolution of equine influenza and the origin of canine influenza. *Proc Natl Acad Sci U S A* **111**, 11175-11180 (2014).

Figure Legends

Figure 1. Proteins associated with EcGFP and with its adhesion incompetent mutant WK-EcGFP. (**A**) Immunofluorescence microscopy of A431 cells expressing the GFP-tagged cadherin (EcGFP) or its adhesion defective mutant (WK-EcGFP) in different genetic backgrounds. EcGFP imaged in the cells with E-cadherin knockout (top panel, EcGFP in Ec-KO); WK-EcGFP imaged in the cells with combined E- and P-cadherin knockout (WK-EcGFP in Ec/Pc-KO); EcGFP imaged in the cells with combined E-cadherin and α-catenin knockout (EcGFP in Ec/αCat-KO); EcGFP imaged in the cells

with combined E-cadherin and p120 knockout (EcGFP in Ec/p120-KO); EcGFP imaged in the cells with combined E-cadherin, β-catenin and plakoglobin knockout (EcGFP in Ec/βCat/Pg-KO). Bar, 10 μm. (**B**) Cell lysates (input) obtained from surface-biotinylated cells shown in **A** were analyzed for GFP and for loading control, β-tubulin (btub). The second parts of the lysates were precipitated using streptavidin agarose (Str-IP) and analyzed for GFP. Note that p120 knockout, in contrast to other manipulations, results in dramatic reduction of both total and cell surface E-cadherin levels. (**C**) Diagram showing the median of spectral counts for each protein identified as associating with cadherin CCC complex in our crosslinking experiment. Protein names (or their gene symbols) are given on the top of the diagram, while the genetic backgrounds of the crosslinking experiments are given to the left of the diagram. Proteins are grouped according to their function (given below the diagram). The group of "Lateral membrane receptors and adaptors" is further split into components of desmosomes (1), focal adhesions (2), transmembrane phosphatase and their adaptors (3), membrane adaptors of PLEKHA family (4), polarity regulators (5), and spectrin cytoskeleton (6). The "Actin cytoskeleton" is split into actin motors (7), actin-binding proteins (8), and actin dynamic regulators (9). The "Signaling components" group includes G protein (10), cortical kinases and phosphatases (11), and intermediates of specific signaling pathways (12). Blue circle indicates proteins previously found in BioID-based classic cadherin proteoms (Guo et al., 2014; Li et al., 2019; Van Itallie et al., 2014).

Figure 2. Characterization of the BMPEO3 adducts of the major CCC proteins and some CAPs. EcGFP and WK-EcGFP cells shown in Fig. 1 were cross-linked using BMPEO3 and their lysates were precipitated using GFP-trap as in proteomics experiments. The resulting precipitates were run on SDS-PAGE, transferred on nitrocellulose and blotted with antibodies specific to E-cadherin (E-cad), β-catenin (β-cat), p120 (p120), α-catenin (α-cat), vinculin (vinculin), and erbin (erbin). Note that in all cases the adducts run as distinct bands. The monomeric form of each protein (including a position for monomeric erbin) is indicated by arrowheads. E-cadherin does not form any adducts since its intracellular region does not have cysteines. Also note that the single vinculin-containing adduct corresponds in size to the one of major β-catenin adduct. The

relative positions of marker proteins, the same for all panels, are indicated at the left margin.

Figure 3. Subcellular localization of erbin and scribble clusters. (**A, B**) Immunofluorescence microscopy of A431 cells expressing the GFP-tagged form of cadherin (green) and Erbin (erb, red, **A**) or Scrib (scrib, red, **B**) in various backgrounds (abbreviations as in Fig. 1A): EcGFP in Ec-KO (EcGFP), WK-EcGFP in Ec/Pc-KO (WK-EcGFP), or EcGFP in Ec-KO cultured for 20 min with the function-blocking E-cadherin mAb SHE78-7 (EcGFP+SHE78-7). The dash line boxed regions indicted in the green images are magnified on the right of each panel (**A, B, E**). The dash line boxed regions in the magnified portions are further enlarged in panel (**C**). (**C**) Cell-cell contact regions showing relative localization for pairs of proteins: E-cadherin and erbin (EcGFP-erb), E-cadherin and Scribble (EcGFP-scrib), Erbin and Scribble (erb-scrib), and E-cadherin and β-catenin as a control (EcGFP-βCat). In all cases but the control (bottom graph), the red clusters only partially correspond to pAJs. The arrow shows one of the AJ-separated erbin or scrib clusters (in EcGFP-erb or EcGFP-scrib) or Scrib-deficient erbin cluster (in erbin-scrin). Line-scans performed along the white lines are shown on the right panel. A.U., arbitrary unit. (**D**) AJ incorporation index (AJ-II), which is defined as the ratio between the area of erbin- or scribble-specific fluorescence of the selected AJs to the total area of the same AJs defined by EcGFP fluorescence. Median values are indicated by horizontal bars, n=15. (**E**) Immunofluorescence microscopy of A431 cells double stained for erbin (erb, green) and Scribble (scrib, red) or for Erbin (erb, green) and Desmoglein-2 (Dsg2, red). Erbin clusters do not correspond to Scribble clusters or to desmosomes. The boxed regions are enlarged on the right panel and further zoomed in panel (**C**). Bars, 10 μm in all figures.

Figure 4: Structural model of E-cluster connected to actin. All components of the 3x3 lattice – E-cadherin, p120, β-catenin and α-catenin (color coded, labelled, and shown in surface representation), satisfy constraints imposed by *cis*- and *trans*-interactions of cadherins (encircled on the right) in the extracellular space (between two cellular membranes denoted as parallelepipeds). Two views of the lattice are shown. The E-

cluster is connected to F-actin (shown in grey surface representation) by ABD domains of α-catenin (red) via flexible linkers. F-actin is positioned in such a way that ABD domains from two adjacent rows of CCC complexes connect to one actin filament by binding the closest available ABD-binding site. The ABD domains in the far-right row of the lattice (dark red) are shown as bound to the rest of α-catenin.

Figure 5. mAb-free and mAb-bound clusters could not be intermixed. (**A**) Immunofluorescence microscopy of A431 cells pulse-labeled with 67A4 mAb. The cells were incubated with the 67A4 mAb for 2 min and were either fixed (67A4 2 min) or were further cultured for 30 min in the antibody-free media (67A4 2 min then N med 30 min). Cells were then stained for β-catenin (βCat) and mouse IgG (mAb). Note that during 2 min-long incubation, the mAb predominantly interacted with extra-junctional cadherin and only then integrated into AJ-associated clusters. Dashed line boxed regions are magnified on the right. Arrows mark mAb-free AJs. Bars, 10 μm. (**B**) Average PCC between β-catenin fluorescence that marks AJs and the mAb-derived fluorescence at different time after addition of the mAb. The error bars represent SEs (n = 10).

Figure 6. Dynamics of the mAb-bound cadherin clusters. (**A**) A single frame taken from the movie S1, see SI Appendix. Immunofluorescence microscopy of A431 cells expressing Dendra2-tagged E-cadherin (EcDn) labeled with the Alexa Fluor 594-conjugated 67A4 mAb for 1 min and then imaged in the mAb-free media at 10 sec resolution for EcDn (green) and for the mAb (red). The presented frame was taken 400 sec after labeling. Bar, 10 μm. (**B**) Magnification of three areas indicated by the dashed line boxed regions in A (numbered) and their time-evolution. Each area is presented in five different ways: EcDn (400) – a single frame of EcDn fluorescence; mAb(400) – a parallel single frame of mAb fluorescence; merge – combined green and red fluorescence of the same frame; EcDn (400+410+420) – three consecutive frames (taken 400, 410 and 420 sec after labeling) of EcDn fluorescence were colorized in red, green and blue (correspondingly) and merged. Note that the combined image is mostly black and white showing that AJs were structurally stable during 20 sec timeframe; mAb (400+410+420) – the same three frames as above but taken in the mAb fluorescence channel were

similarly colorized and merged. Note that mAb-bound E-cadherin clusters are multicolored showing their high dynamics. Bars, 5 μm. (**C**) A431Ec-KO cells expressing adhesion incompetent W-EcDn mutant were fixed and imaged for W-EcDn using Dendra2 fluorescence (Dn) in standard culture (W-EcDn) or after 40 min with 67A4 mAb (W-EcDn+ mAb, 40 min). In latter case the cells were stained for mouse IgG (mAb). Note that in both cultures the W-EcDn mutant is unable to form AJ. Bars, 10 μm. (**D**) A431Ec-KO cells expressing W-EcDn mutant were labeled and imaged as indicated in (A). Single frames of the W-EcDn (W-EcDn) and the mAb (mAb) fluorescence taken 300 sec after labeling are shown in the upper panel. Note that the mutant and the mAb do not show specific enrichment in the cell-cell contact. The bottom panel presents the overlay of three consecutive frames of W-EcDn and the mAb fluorescence, W-EcDn (300+310+320) and mAb (300+310+320), correspondingly, were processed as in (B). Only the area indicated by a dashed box in W-EcDn is shown. Bar, 10 μm (**E**) Immunofluorescence microscopy of E-cadherin in α-catenin depleted A431 cells (αCat-sh) using an anti-cadherin antibody. Note that cadherin cannot form well-defined AJs in these cells. Bar, 10 μm. (**F**) A single time-lapse DIC image (DIC) of α-catenin-depleted A431 cells taken 300 sec after the cells were labeled by 67A4 mAb as indicated in A; mAb (300) - the mAb fluorescence of the area indicated by a dashed box 300 sec after labeling; mAb (300+310+320) - three consecutive frames of the mAb fluorescence processed as in (B). Bar, 10 μm.

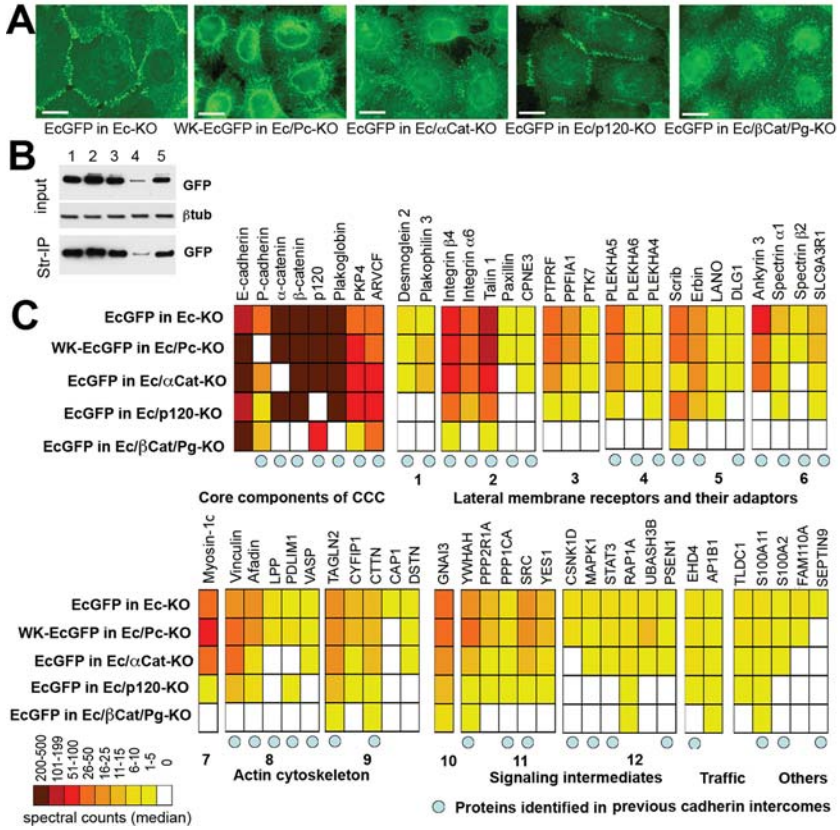
A
EcGFP in Ec-KO
WK-EcGFP in Ec/Pc-KO
EcGFP in Ec/αCat-KO
EcGFP in Ec/p120-KO
EcGFP in Ec/βCat/Pg-KO
B
1 2 3 4 5
input
GFP
βtub
Str-IP
GFP
C
EcGFP in Ec-KO
WK-EcGFP in Ec/Pc-KO
EcGFP in Ec/αCat-KO
EcGFP in Ec/p120-KO
EcGFP in Ec/βCat/Pg-KO
E-cadherin
P-cadherin
α-catenin
β-catenin
p120
Plakoglobin
PKP4
ARVCF
Desmoglein 2
Plakophilin 3
Integrin β4
Integrin α6
Talin 1
Paxillin
CPNE3
PTPRF
PPFIA1
PTK7
PLEKHA5
PLEKHA6
PLEKHA4
Scrib
Erbin
LANO
DLG1
Ankyrin 3
Spectrin α1
Spectrin β2
SLC9A3R1
1
2
3
4
5
6
Core components of CCC
Lateral membrane receptors and their adaptors
Myosin-1c
Vinculin
Afadin
LPP
PDLIM1
VASP
TAGLN2
CYFIP1
CTTN
CAP1
DSTN
GNAI3
YWHAH
PPP2R1A
PPP1CA
SRC
YES1
CSNK1D
MAPK1
STAT3
RAP1A
UBASH3B
PSEN1
EHD4
AP1B1
TLDC1
S100A11
S100A2
FAM110A
SEPTIN9
7
8
9
10
11
12
Actin cytoskeleton
Signaling intermediates
Traffic
Others
Proteins identified in previous cadherin intercomes
200-500
101-199
51-100
26-50
16-25
11-15
6-10
1-5
0
spectral counts (median)

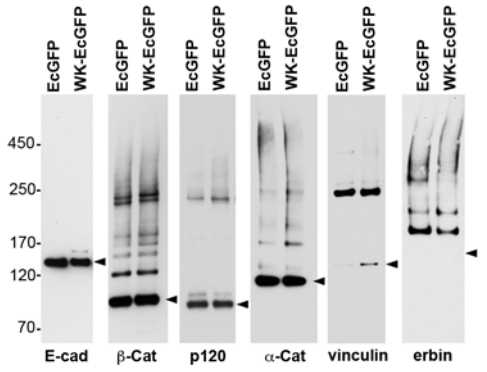
EcGFP
WK-EcGFP
450-
250-
170-
120-
70-
E-cad
β-Cat
p120
α-Cat
vinculin
erbin

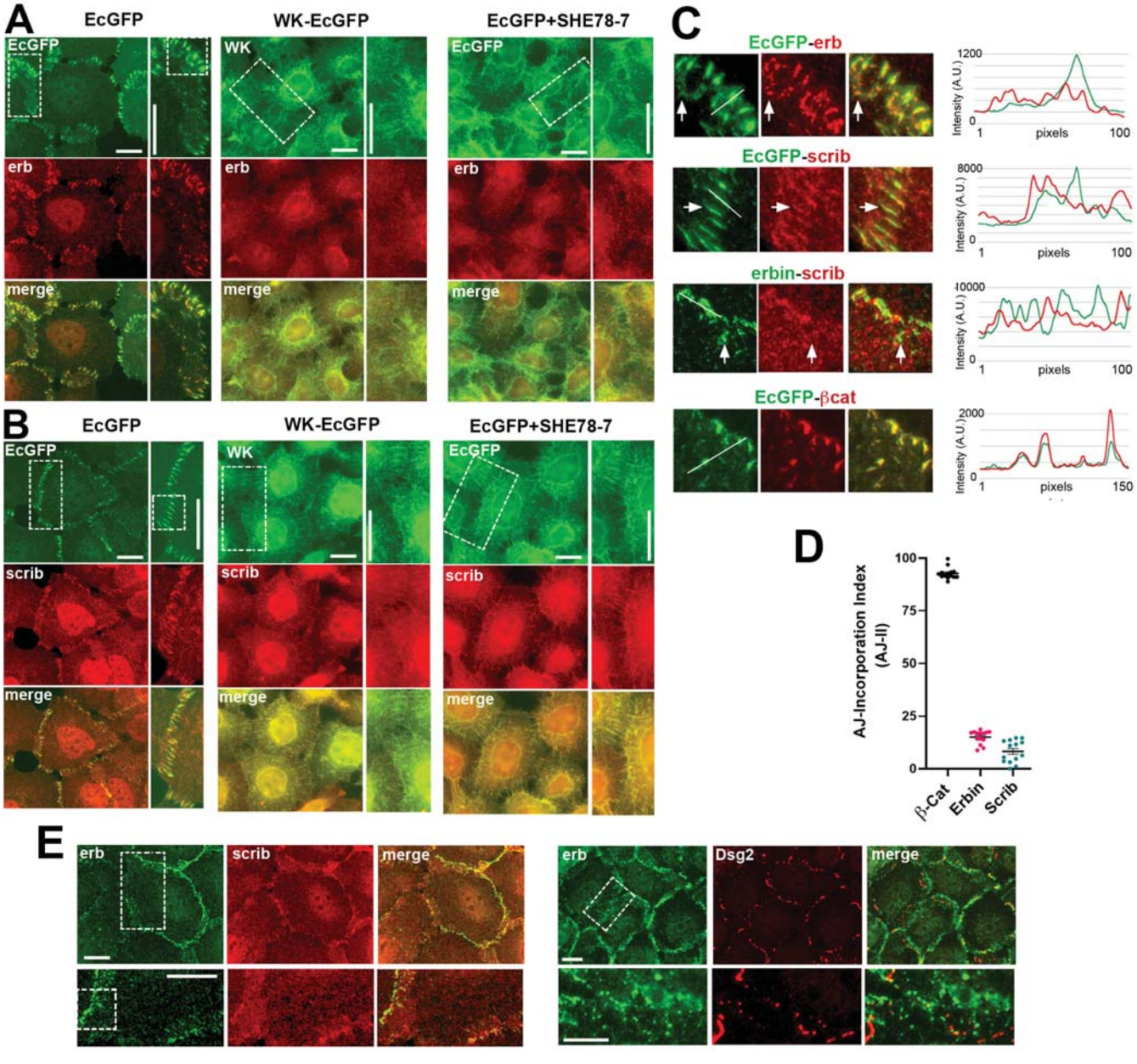
A
EcGFP
WK-EcGFP
EcGFP+SHE78-7
EcGFP
WK
erb
merge
B
scrib
C
EcGFP-erb
EcGFP-scrib
erbin-scrib
EcGFP-βcat
Intensity (A.U.)
pixels
D
AJ-Incorporation Index (AJ-II)
β-Cat
Erbin
Scrib
E
Dsg2

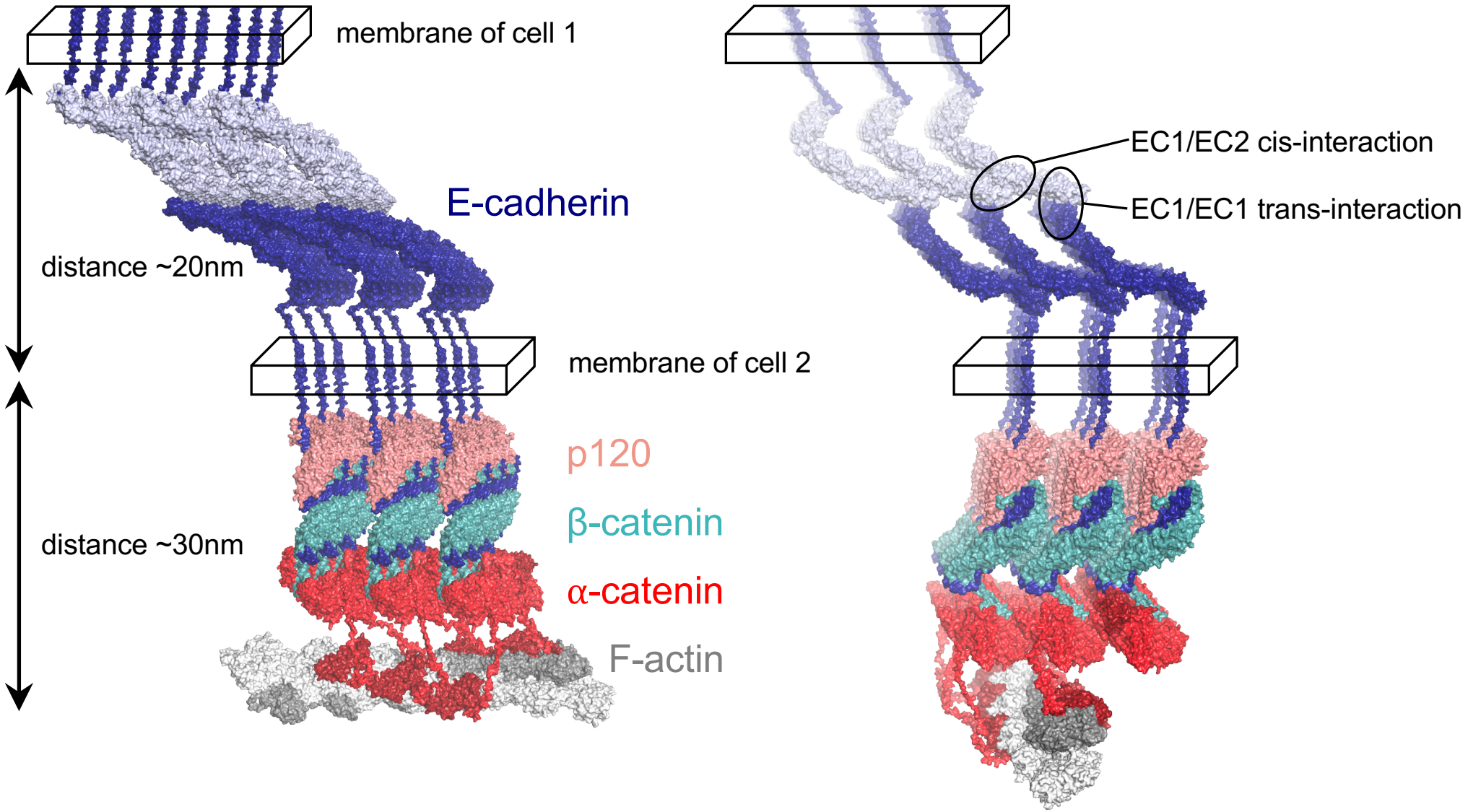
membrane of cell 1
E-cadherin
distance ~20nm
membrane of cell 2
p120
β-catenin
distance ~30nm
α-catenin
F-actin
EC1/EC2 cis-interaction
EC1/EC1 trans-interaction

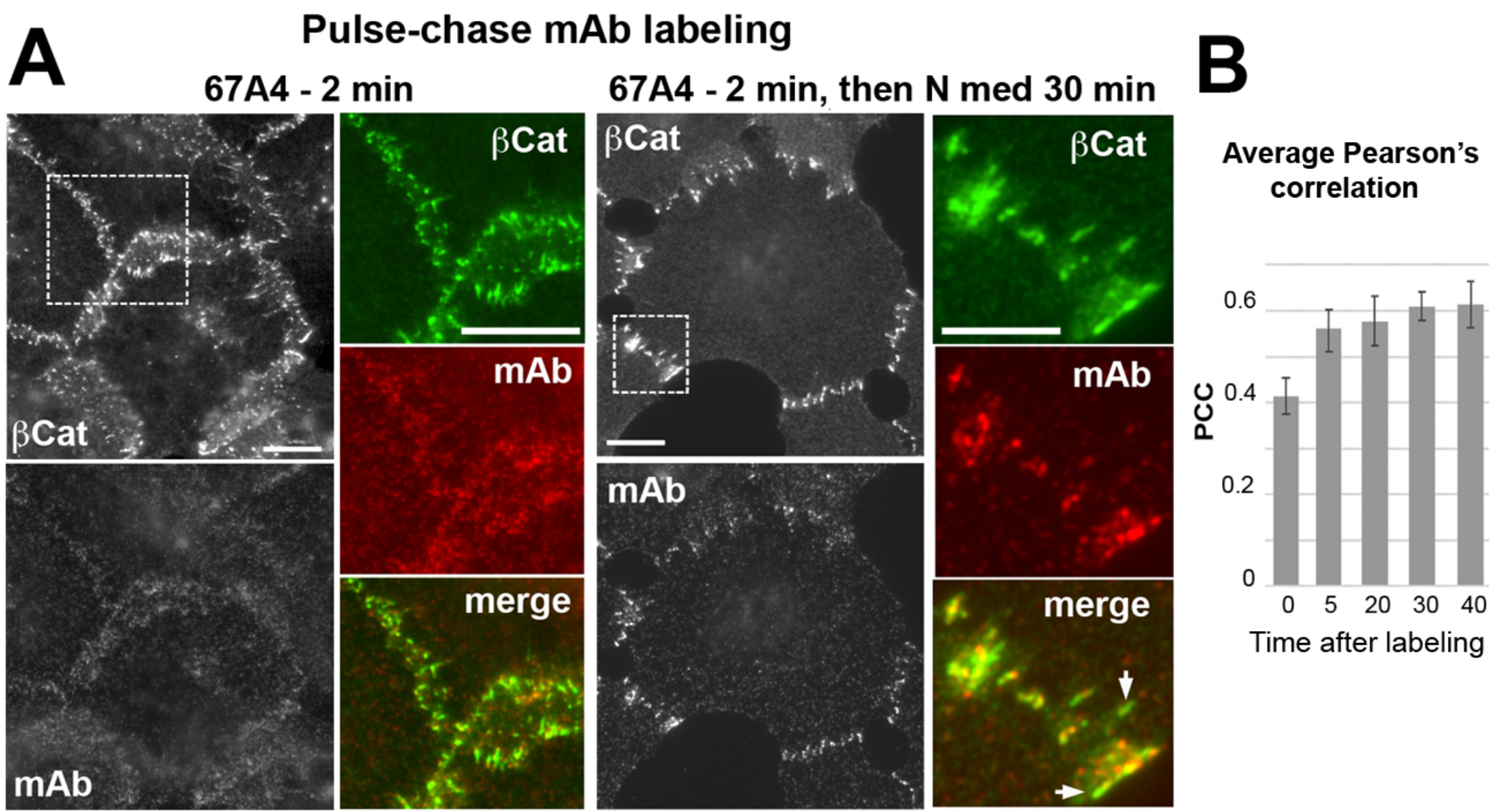
A
Pulse-chase mAb labeling
67A4 - 2 min
67A4 - 2 min, then N med 30 min
βCat
mAb
merge
B
Average Pearson's correlation
PCC
0
0.2
0.4
0.6
0
5
20
30
40
Time after labeling

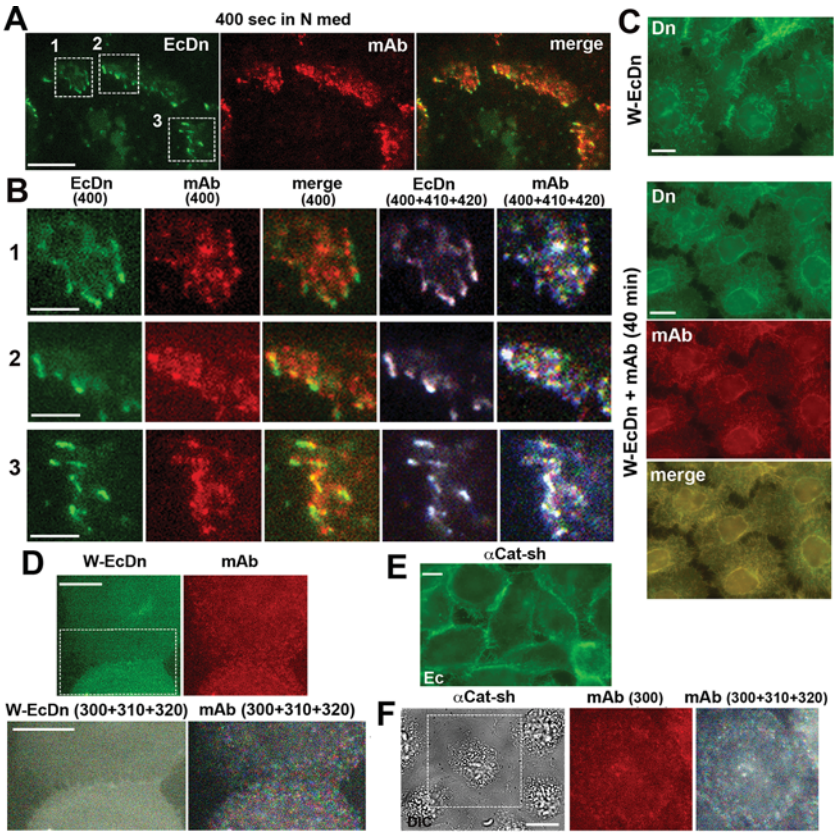
A
400 sec in N med
1
2
3
EcDn
mAb
merge
B
EcDn (400)
mAb (400)
merge (400)
EcDn (400+410+420)
mAb (400+410+420)
1
2
3
C
W-EcDn
Dn
W-EcDn + mAb (40 min)
Dn
mAb
merge
D
W-EcDn
mAb
W-EcDn (300+310+320)
mAb (300+310+320)
E
αCat-sh
Ec
F
αCat-sh
mAb (300)
mAb (300+310+320)
DIC

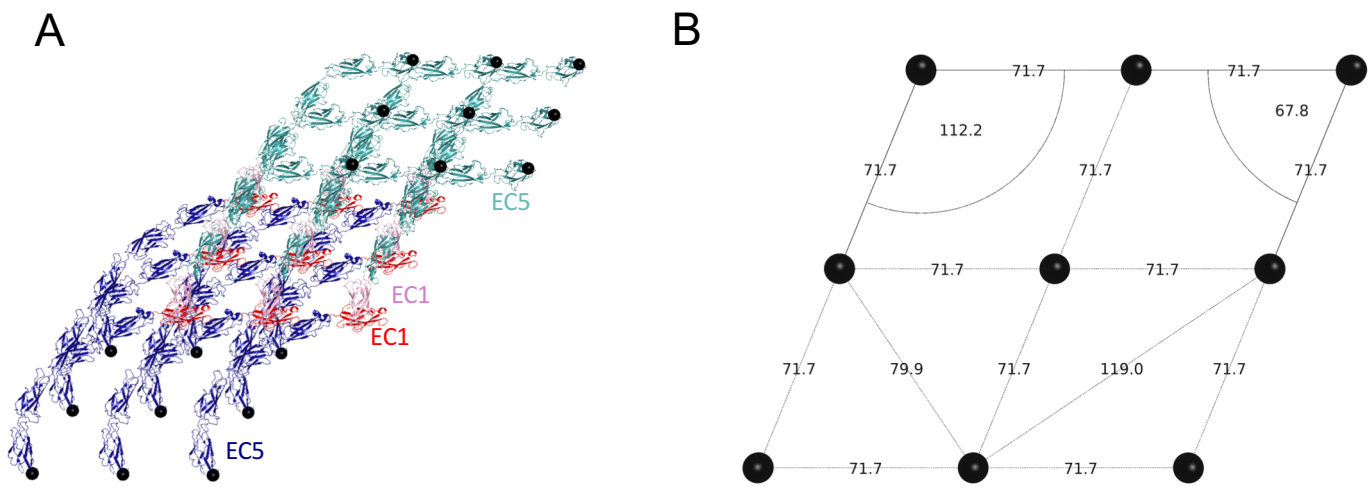

Figure S1

Extracellular cadherin lattice imposes constraints on cytoplasmic components. (**A**) 3x3 lattice formed by *cis*- and *trans*- interactions of E-cadherin ectodomains (blue or cyan) in ribbon representation. EC1 domains that interact in trans are highlighted in red or pink. The N-terminal (EC1) and the C-terminal (EC5) extracellular domains are marked for one cadherin *trans*-dimer. Ca atoms at the C-terminal of EC5 domains are shown as black dots. (**B**) Distances (in Å) and angles (in °) between Ca atoms denoted as dots define spatial constraints imposed by cadherin *cis*- and *trans*- interactions on cytoplasmic components.

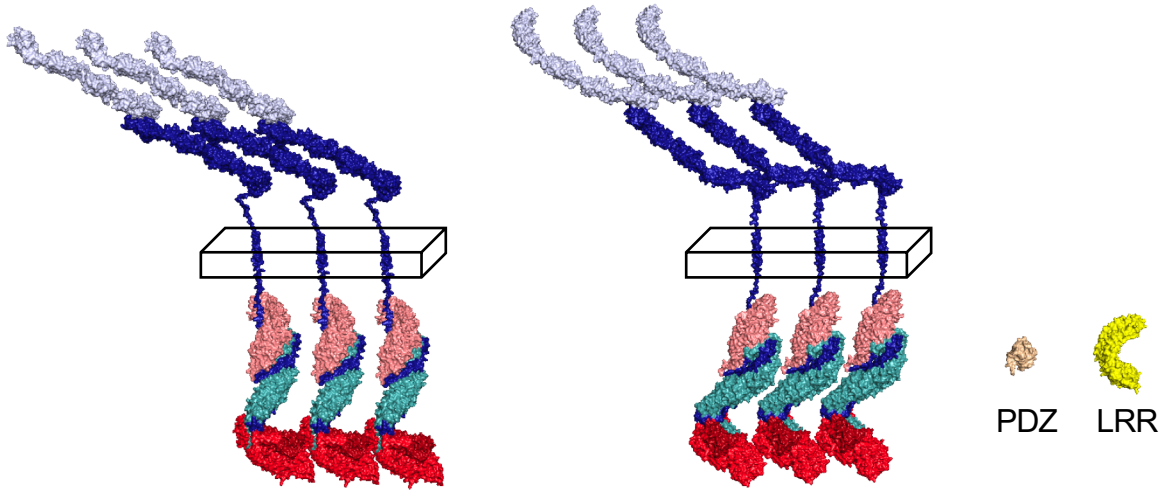

Figure S2

Visual size comparison of erbin and scribble protein domains with lattice spacings. Two 3x1 lattices along two distinct dimensions of the 3x3 lattice in Fig. 4 are shown alongside PDZ and LRR domains, all in surface representations and arranged at the same distance to the observer to demonstrate relative sizes of the proteins with respect to the lattice spacings. A PDZ domain (orange, PDBID 5VWC) would barely fit into the lattice, while LRR domain (yellow, PDBID 4U09) would not fit. All other notations and colors as in Fig. 4.

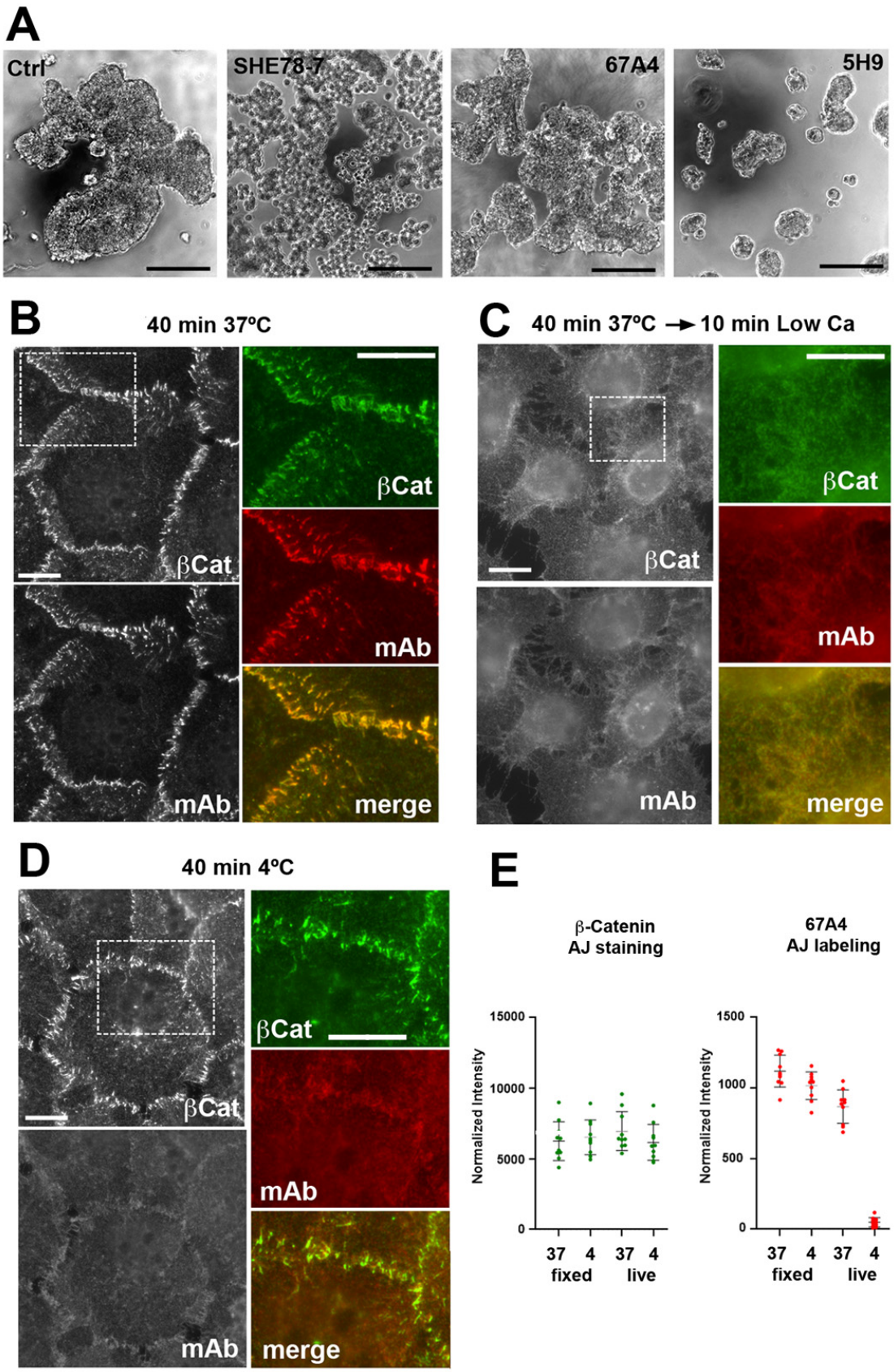

Figure S3

mAbs 67A4 and 5H9 do not block cadherin adhesion. See full caption on the next page

Figure S3

mAbs 67A4 and 5H9 do not block cadherin adhesion. (**A**) Hanging drop assay with A431 cells in standard media (Ctrl), in the presence of adhesion-blocking SHE78-7 (SHE78-7) or adhesion-neutral 67A4 (67A4) or 5H9 (5H9) mAbs. Note that the "neutral" mAbs failed to inhibit formation of compact cell aggregates. Bars, 0.5 mm. (**B**) Immunofluorescence microscopy of A431 cells cultured for 40 min with 67A4 mAb at 37 ºC. Cells were then stained with rabbit β-catenin antibody to reveal AJs (bCat) and with mouse IgG antibody to detect 67A4-bound E-cadherin (mAb). Bar, 10 mm. (**C**) The parallel cell culture, after 40 min with the mAb as in B, was incubated for additional 10 min with 67A4 mAb in low calcium media. Complete dissolution of mAb-bound AJs indicates that the mAb does not cross-link cadherin through adjacent cells. Bar, 10 mm. (**D**) The same experiment as in B but performed at 4ºC. Note that AJs remain unlabeled in metabolically inactive cells. The dash line boxed regions (B-D) are magnified on the right of each panel. To show the distribution of mAb on the cell surface, the exposure time for mAb staining in D was twice longer than that in B and C. Bar, 10 mm. (**E**) Quantification of the 67A4 mAb incorporation into AJs at 4°C and 37°C in fixed and live cells. Fixed and permeabilized A431 cells (fixed) were stained with rabbit β-catenin antibody (β-catenin AJ staining) or with mouse 67A4 mAb (67A4 AJ labeling) at 4°C or 37°C and then stained with the corresponding secondary antibodies at RT. Live cells (live) were cultured for 40 min with the mAb before fixation, and then stained for β-catenin and for the mouse IgG. Note, the staining of AJs in fixed cells is temperature-independent. In live cells, by contrast, the mAb incorporates into AJs only at 37°C.

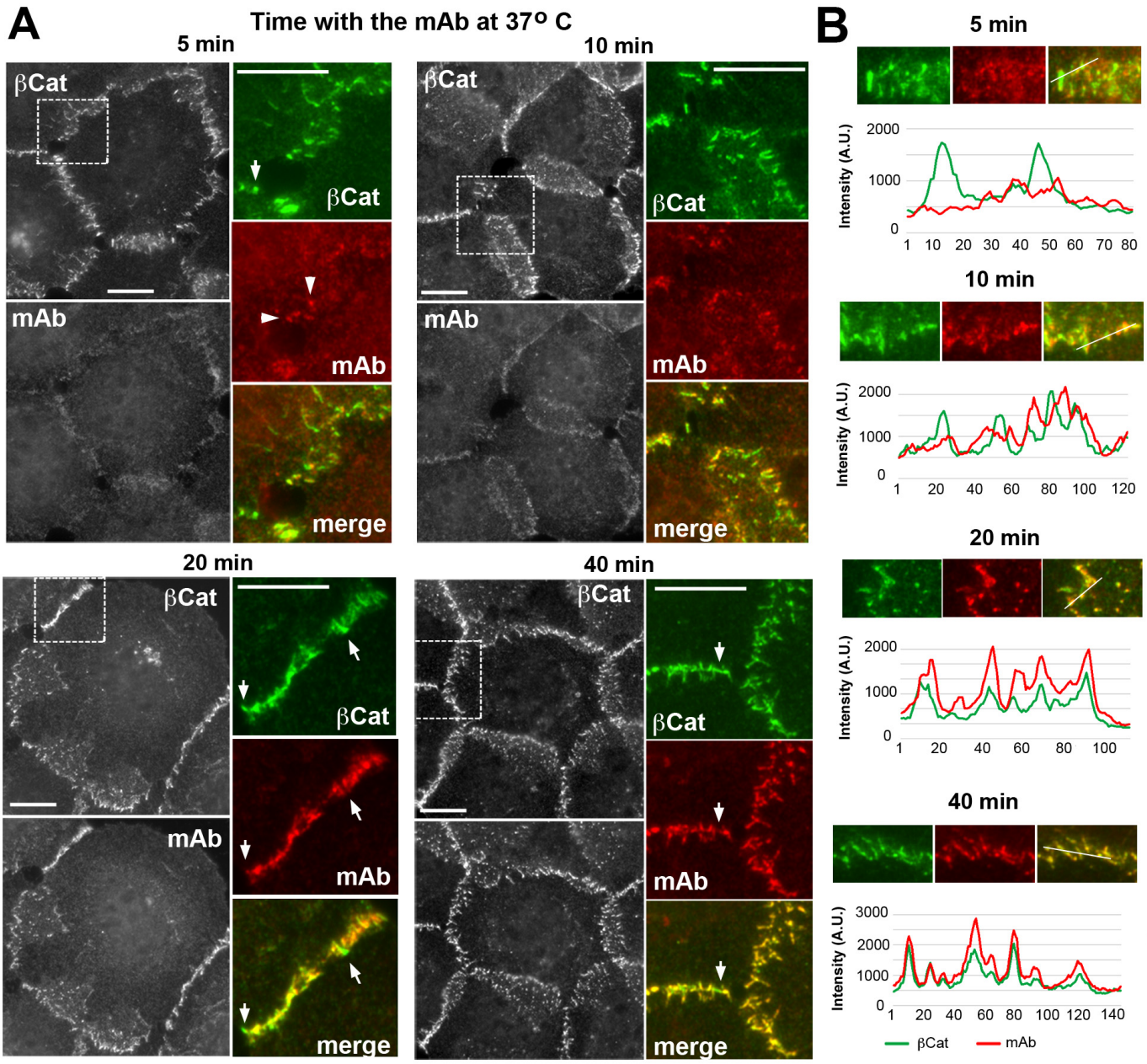

Figure S4

67A4 mAb integrates into the junctions through junction reassembly. (**A**) A431 cells were cultured with 67A4 mAb at 37ºC for 5, 10, 20, or 40 minutes. Cells were then stained for β-catenin (bCat) and for mouse IgG (mAb) as indicated in Fig. 5. Note that mAb-containing clusters gradually replace the unlabeled AJs. Arrowheads show two of the mAb-bound cadherin clusters formed 5 min after addition of the mAb. Arrows show mAb-free AJs after 20 and 40 min in the mAb-containing media. Dashed line boxed regions are magnified on the right. Bars, 10 mm. (**B**) A line scan analysis of the mAb-bound clusters performed along the lines (their lengths are shown in pixels in the graphs) shown in the merge images. The time after the addition of the mAb is indicated. Note that the similarities between mAb and E-cadherin distribution is gradually increasing over time.

A

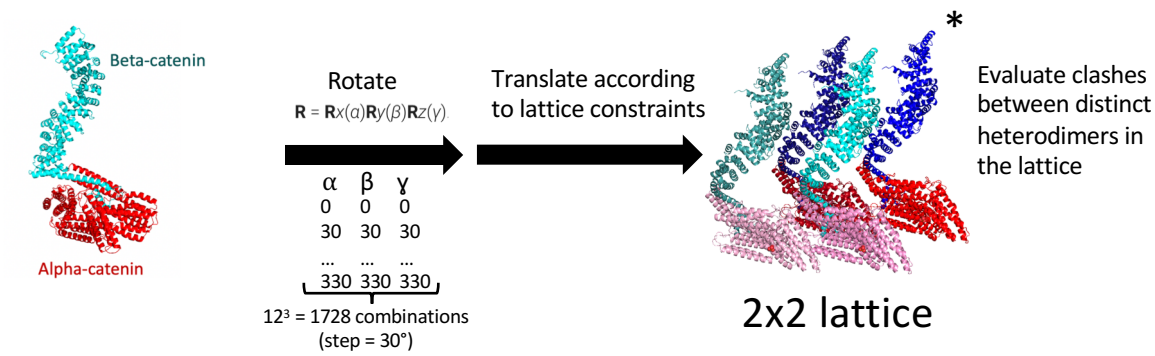

B

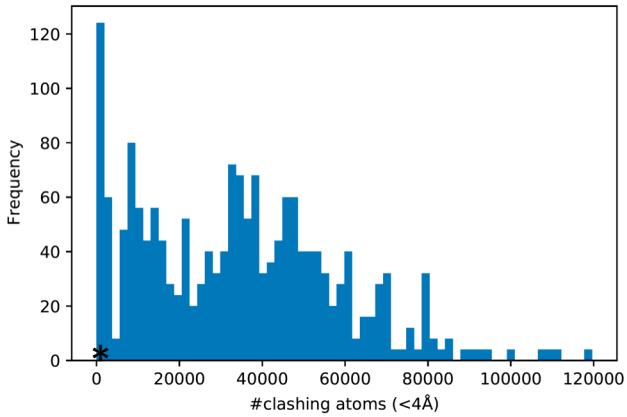

C

atom NH1 (ARG137, chain A) clashes with atom NZ (LYS577, chain C), d =3.9 Å
atom NH1 (ARG137, chain B) clashes with atom NZ (LYS577, chain D), d =3.9 Å
atom NZ (LYS577, chain C) clashes with atom NH1 (ARG137, chain A), d =3.9 Å
atom NZ (LYS577, chain D) clashes with atom NH1 (ARG137, chain B), d =3.9 Å

Figure S5

Finding orientation of a full-length α-catenin/β-catenin with no clashes in the lattice. (**A**) Model of full-length α-catenin/β-catenin heterodimer built from crystal structure fragments in ribbon representation followed by a flow chart to generate 2x2 lattices using rotations by different Euler angle combinations and subsequent evaluation of clashes. (**B**) Distribution of clashes found in 1728 2x2 lattices. (**C**) List of closest atoms in the lattice with minimal number of clashes. This lattice, denoted with asterisk, was used in the final model.

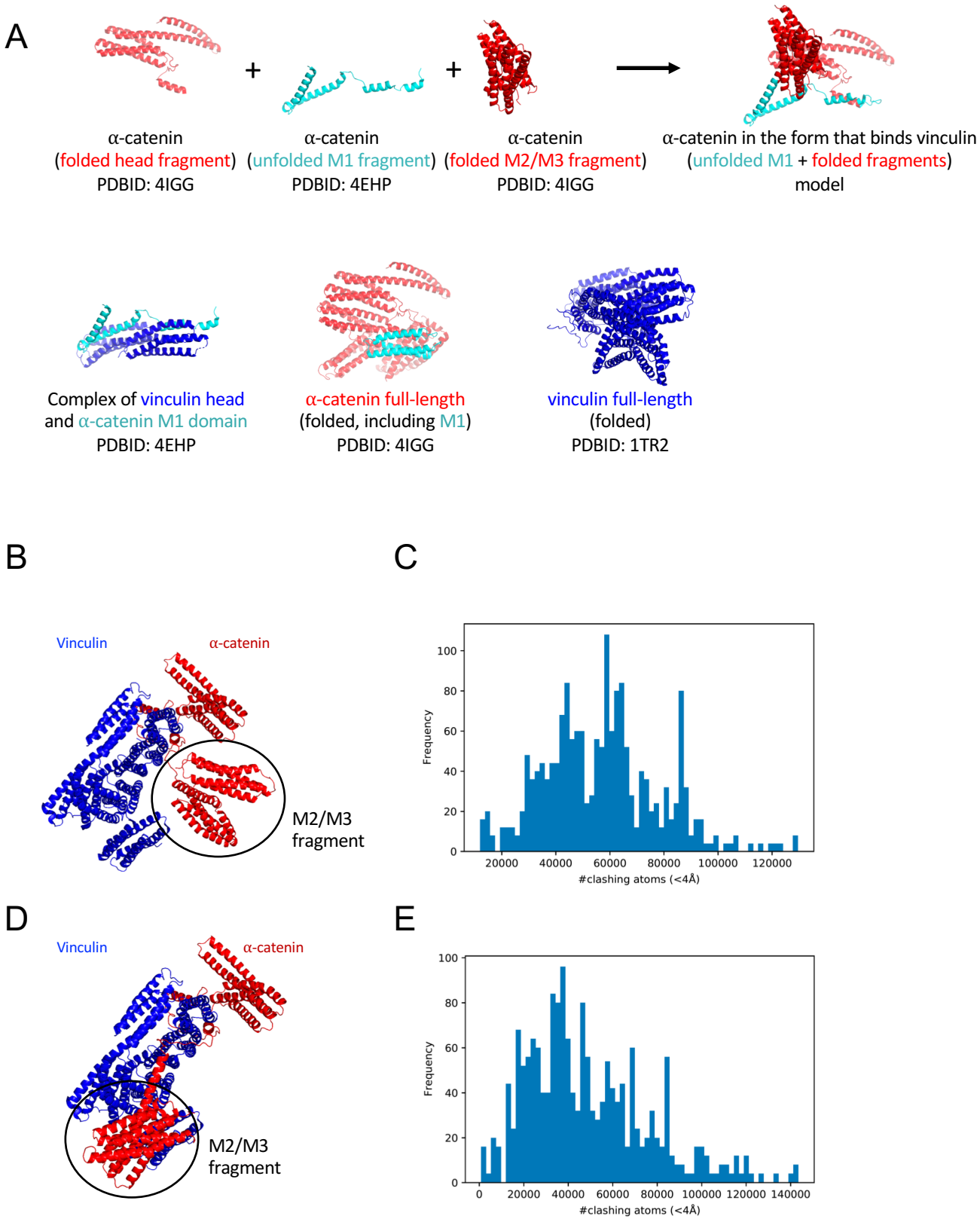

Figure S6

Vinculin is unlikely to form an interspersed lattice with α-catenin in E-clusters. (**A**) Model of α-catenin in the form to bind vinculin and crystal structure fragments (with PDBIDs given in parenthesis) used to build the model, all in ribbon representation. Head domain of full-length α-catenin was stitched to an unfurled M1-domain of α-catenin from the complex with vinculin, and further to the M2/M3 fragment of full-length α-catenin (top panel). The reference crystal structures used to build the model are shown in the bottom panel. (**B**) α-catenin/vinculin heterodimer model in ribbon representation obtained by merging full-length vinculin structure and α-catenin in the form to bind vinculin from (A). (**C**) Distribution of clashes found in 1728 2x2 lattices built by rotating the heterodimer in (B) by different combinations of Euler angles (from a,β,ɣ=0° to a,β,ɣ =330° with a stepsize of 30°. (**D**) same as B but with reoriented M2/M3 fragment - a more compact model. (**E**) Distribution of clashes found in 1728 2x2 lattices built by rotating heterodimer in (D).

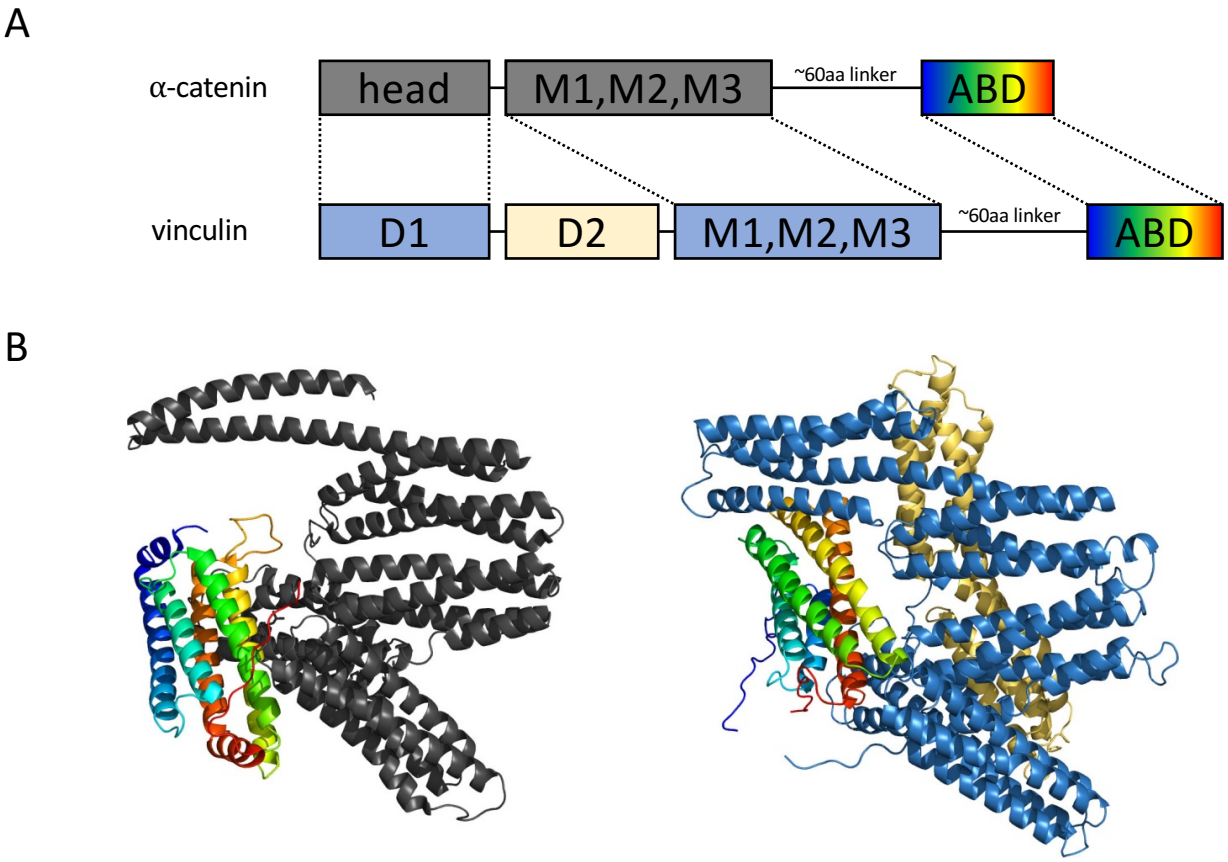

Figure S7

Structural similarity of α-catenin and vinculin. (A) Schematic representation and similarities of domain composition between α-catenin and vinculin. Structurally similar domains are connected by dotted lines. Both proteins can bind actin via ABD (rainbow), which is connected via long and flexible linker to M domain. Vinculin has an extra domain, D2 in yellow, not present in α-catenin. (B) Ribbon representation of aligned full-length α-catenin (PDBID: 4IGG) and vinculin (PDBID: 1TR2) structures. Color code of protein domains as in (A).

			Mean protein spectra counts for cells:					Statistics for EcGFP	
#	Gene	Protein name	EcGFP	WK-EcGFP	□Cat-KO	p120-KO	Pg/□Cat-KO	stand dev	p value
1	CTNNA1	Catenin Alpha 1	390	388	0	313	0	39.42805383	0.00000010
2	CTNNB1	Catenin Beta 1	372	315	305	184	0	98.23441352	0.00002865
3	CTNND1	Catenin Delta 1	244	235	232	0	61	28.91201760	0.00000026
4	JUP	Plakoglobin	239	343	276	210	0	136.91359806	0.00181053
5	CDH1	E-Cadherin	151	245	410	181	287	51.13000000	0.00018769
6	TLN1	Talin 1	127	136	94	35	3	27.78403104	0.00000952
7	ITGB4	Integrin Subunit Beta 4	61	82	67	30	1	12.30756639	0.00000598
8	ANK3	Ankyrin 3	58	35	39	0	0	13.91470616	0.00001725
9	MYO1C	Myosin IC	49	59	31	5	0	9.87782509	0.00000583
10	PKP4	Plakophilin 4	49	52	51	76	9	18.07260489	0.00017676
11	ARVCF	ARVCF Delta Catenin Family Member	48	48	65	61	45	18.59979519	0.00023093
12	SCRIB	Scribble	41	46	9	27	6	11.88436348	0.00005057
13	PLEKHA5	Pleckstrin Homology Domain Containing A5	41	31	25	8	0	15.69349274	0.00024000
14	CDH3	P-Cadherin	34	0	22	8	14	11.20799035	0.00009320
15	ITGA6	Integrin Subunit Alpha 6	30	31	26	11	0	9.29925752	0.00007282
16	GNAI3	G Protein Subunit Alpha I3	26	30	22	12	8	5.53774924	0.00000831
17	PTPRF	Protein Tyrosine Phosphatase Receptor Type F	26	33	22	4	0	12.15181742	0.00065298
18	ERBIN	Erbb2 Interacting Protein (erbin)	23	19	19	11	0	8.36660027	0.00017189
19	YWHAH	Tyrosine 3-Monooxygenase/Tryptophan 5-Monooxygenase Activation Protein Eta	22	26	13	4	2	6.28300808	0.00004638
20	VCL	Vinculin	21	28	29	11	0	9.74435123	0.00056641
21	TAGLN2	Transgelin 2	21	19	17	14	4	4.82059076	0.00001387
22	PPFIA1	PTPRF Interacting Protein Alpha 1	18	18	7	5	0	5.22812905	0.00004918
23	AFDN	Afadin	17	25	7	7	0	5.95618926	0.00013363
24	SRC	Non-Receptor Tyrosine Kinase	17	19	15	4	0	4.64962876	0.00003036
25	SLC9A3R1	SLC9A3 Regulator 1	14	12	8	4	0	2.91138978	0.00000768
26	CYFIP1	Cytoplasmic FMR1 Interacting Protein 1	14	14	2	4	0	7.15807902	0.00093239
27	SPTAN1	Spectrin Alpha	13	2	1	5	0	6.39940473	0.00072180
28	YES1	YES Proto-Oncogene 1	12	13	8	3	0	4.94734176	0.00031723
29	PPP2R1A	Protein Phosphatase 2 Scaffold Subunit Aalpha	12	12	4	5	0	5.09434794	0.00032760
30	EHD4	EH Domain Containing 4	10	9	10	3	0	5.06152621	0.00079280
31	SPTBN1	Spectrin Beta	9	1	0	0	0	10.88467687	0.03740228
32	PPP1CA	Protein Phosphatase 1 Catalytic Subunit Alpha	8	10	5	4	0	5.74041644	0.00649435
33	LPP	LIM Domain Containing Preferred Translocation Partner In Lipoma	7	7	0	0	0	2.30940108	0.00010037
34	CSNK1D	Casein Kinase 1 Delta	7	7	0	0	0	2.47847880	0.00013266
35	PLEKHA6	Pleckstrin Homology Domain Containing A6	7	8	10	0	0	3.81725406	0.00116710
36	TLDC1	LysM-associated domain containing 1	6	10	4	2	0	1.67616342	0.00003452
37	MAPK1	Mitogen-Activated Protein Kinase 1	6	3	2	0	0	3.81725406	0.00372336
38	S100A11	S100 Calcium Binding Protein A11	6	6	4	3	4	1.27241802	0.00001245
39	STAT3	Signal Transducer And Activator Of Transcription 3	6	6	3	0	0	3.95209408	0.00486935
40	DSG2	Desmoglein 2	6	5	4	0	0	4.59813627	0.00614967
41	RAP1A	RAP1A	6	7	7	4	2	2.03540098	0.00013376
42	UBASH3B	Ubiquitin Associated And SH3 Domain Containing B	6	11	5	0	0	4.52506248	0.00574050
43	FAM110A	Family With Sequence Similarity 110 Member A	6	4	0	0	0	2.23606798	0.00019614
44	CPNE3	Copine 3	5	5	2	0	0	2.57275098	0.00070159
45	LRRC1	Leucine Rich Repeat Containing 1	5	5	2	0	0	2.99205297	0.00339240
46	SEPTIN9	Septin 9	5	0	0	0	0	3.38765265	0.00349303
47	DLG1	Discs Large MAGUK Scaffold Protein 1	5	5	3	0	0	3.65148372	0.00552972
48	PSEN1	Presenilin 1	5	5	4	0	0	1.60356745	0.00006284
49	PDLIM1	PDZ And LIM Domain 1	5	6	0	3	0	2.91138978	0.00170927
50	CTTN	Cortactin	4	4	2	0	0	2.54483604	0.00351881
51	CAP1	Cyclase Associated Actin Cytoskeleton Regulatory Protein 1	4	0	0	0	0	3.40168026	0.00787071
52	PKP3	Plakophilin 3	4	12	15	0	0	1.34518542	0.00009186
53	DSTN	Destrin	4	2	1	0	0	1.61834719	0.00017624
54	VASP	Vasodilator Stimulated Phosphoprotein	4	5	4	0	0	2.58198890	0.00318304
55	PLEKHA4	Pleckstrin Homology Domain Containing A4	4	10	6	4	0	2.88675135	0.00525169
56	AP1B1	Adaptor Related Protein Complex 1 Subunit Beta 1	3	5	5	1	3	1.39727626	0.00139858
57	PXN	Paxillin	3	4	0	0	0	1.34518542	0.00067816
58	PTK7	Protein Tyrosine Kinase 7	2	3	4	0	0	2.62769136	0.03049066
59	S100A2	S100 Calcium Binding Protein A2	2	1	1	0	0	1.61834719	0.00368203

Core Components of Cadherin-Catenin Complex	
Lateral Membrane Receptors and their Adaptors	
Actin Cytoskeleton	
Signaling Intermediates	
Traffic	
Others	

Table S1

Proteins identified in anti-GFP precipitates.

Movie S1. Dynamics of the mAb-bound E-cadherin clusters. A431 cells expressing EcDn were briefly stained with the Alexa Fluor 594-conjugated 67A4 mAb and then immediately imaged simultaneously in green and red channels. Images were acquired at 10 sec intervals.